Am J Cancer Res 2022;12(10):4520-4544
www.ajcr.us /ISSN:2156-6976/ajcr0143438

Original Article

CDH13 is a prognostic biomarker and a potential therapeutic target for patients with clear cell renal cell carcinoma

Yuan Shao[2,4*], Wenxia Li[3,4*], Lin Zhang[4*], Bo Xue[4], Yongquan Chen[4], Zikuan Zhang[4], Dongwen Wang[4,5], Bo Wu[1]

[1]Department of Urology, First Hospital of Shanxi Medical University, Taiyuan 030001, Shanxi, China; [2]Department of Urology, The Second Hospital of Tianjin Medical University, Tianjin 300070, China; [3]Clinical College of Neurology, Neurosurgery and Neurorehabilitation, Tianjin Medical University, Tianjin 300350, China; [4]Shanxi Medical University, Taiyuan 030001, Shanxi, China; [5]National Cancer Center/National Clinical Research Center for Cancer/Cancer Hospital & Shenzhen Hospital, Chinese Academy of Medical Sciences and Peking Union Medical College, Shenzhen 518116, Guangdong, China. [*]Equal contributors.

Received April 10, 2022; Accepted September 15, 2022; Epub October 15, 2022; Published October 30, 2022

Abstract: CDH13 is an atypical member of the cadherin family and is closely related to the clinicopathological factors and prognosis of many types of cancer. However, the role of CDH13 in clear cell renal cell carcinoma (ccRCC) remains unknown. Therefore, we comprehensively analyzed the expression level, diagnostic efficacy, clinical significance, prognostic value, immune infiltration, methylation status, genetic alteration, and biological functions of CDH13 in ccRCC patients. The results showed that CDH13 was significantly upregulated in ccRCC and strongly correlated with better survival, lower cancer stages, and lower tumor grades of ccRCC patients. Additionally, the immune infiltration analysis indicated that CDH13 might play a crucial role in regulating the tumor microenvironment of ccRCC. The results of methylation analysis showed that the epigenetic status of CDH13 was altered, and the prognosis of ccRCC patients was related not only to DNA methylation but also to m6A modification of CDH13. Finally, the results based on clinical samples further elucidated the expression pattern of CDH13 in ccRCC. In conclusion, CDH13 might be a novel prognostic biomarker and therapeutic target for patients with ccRCC. And our study provides new insights into the potential molecular changes and strategies for the treatment of ccRCC.

Keywords: CDH13, T-cadherin, ccRCC, biomarker, prognosis, methylation, tumor microenvironment

Introduction

Renal cell carcinoma (RCC) is a common malignancy of the urinary system and represents around 2-3% of all cancers, just after prostate cancer and bladder cancer [1-3]. Clear cell renal cell carcinoma (ccRCC) is the main pathological type of RCC, accounting for 70-85% of all RCCs [4, 5]. Early-stage kidney cancer is usually asymptomatic, and more than 50% of RCCs are detected incidentally by non-invasive imaging while investigating various non-specific symptoms and other abdominal diseases [6-8]. As it is invasive and insensitive to radiotherapy and chemotherapy, surgery is the primary strategy for treating patients with localized RCC and locally advanced RCC [9, 10]. However, 20-30% of RCC patients experience tumor recurrence and metastasis after surgery, and the prognosis is poor [11, 12]. Currently, effective and reliable biomarkers are not known other than imaging for the early diagnosis of RCC [13-15]. Moreover, renal tumor biopsy is limited by sampling error and potential complications [16, 17]. Therefore, reliable biomarkers for early diagnosis, risk stratification, and clinical management need to be urgently identified and developed to improve the prognosis of ccRCC patients.

CDH13 is an atypical member of the cadherin superfamily located on human chromosome 16q24, which is a recognized region of oncogenic modification for several types of cancer [18, 19]. Due to the absence of transmembrane domains and intracellular structures, which are generally present in classical cadherin, CDH13

is also known as Truncated cadherin (T-cadherin) [20, 21]. Classical cadherin is mainly distributed at the site of intercellular contact, whereas CDH13 is distributed throughout the cell surface [19, 21, 22]. And this unique structure and distribution suggest that CDH13 not only acts as an intercellular adhesion molecule, but also might act as a signaling receptor involved in the regulation of cellular signaling pathways [23, 24]. With continuous researches, current studies have confirmed that CDH13 plays a critical role in tumor neovascularization, apoptosis, cell cycle, and cell proliferation [22, 25]. The abnormal expression of CDH13 is also closely related to the development of various malignancies, clinicopathological factors, and the prognosis of cancer patients [26-28]. Lin et al. performed immunohistochemical staining to determine the expression level of CDH13 in 113 bladder cancer and 37 normal tissue specimens [26]. The results showed that the expression level of CDH13 in the bladder cancer tissues was lower than that in the normal tissues. Also, CDH13 was closely related to clinicopathological factors, such as the stage and grade of bladder tumors and tumor recurrence, which might be used as a biomarker for predicting the malignancy of bladder cancer [26]. In addition, Wang et al. found that the expression level of CDH13 in oral squamous cell carcinoma tissues was significantly lower than that in the normal tissues and was strongly correlated with the clinicopathological features and the prognosis of patients with oral squamous cell carcinoma [27]. Further mechanistic studies showed that CDH13 might affect cell proliferation through the PI3K/AKT/mTOR signaling pathway [27]. In a study on pancreatic cancer, CDH13 was found to be significantly downregulated in pancreatic cancer tissues and cell lines [28]. And the overexpression of CDH13 was shown to inhibit the activation of the Wnt/β-catenin signaling pathway by regulating epithelial-mesenchymal transition (EMT), thus influencing the proliferation, migration, and invasion of cancer cells [28].

However, the expression level and prognostic value of CDH13 in ccRCC are not known, and the relationship between CDH13 and the clinicopathological features of ccRCC patients has not been investigated. Additionally, the clinical value and the mechanism of action of CDH13 in ccRCC remain unclear. Therefore, in this study, the expression level, diagnostic efficacy, prognostic value, immune infiltration, methylation status, genetic alteration, and function enrichment of CDH13 in ccRCC were comprehensively analyzed by applying bioinformatics. Furthermore, the results of the bioinformatic analysis were also validated by using clinical specimens to comprehensively determine the clinical role of CDH13 as a prognostic biomarker and a potential therapeutic target in ccRCC patients.

Materials and methods

Pan-cancer analysis of CDH13

Oncomine (www.oncomine.org) is a public and comprehensive oncogene data-mining platform, which includes results of transcriptional expression from 20 common neoplasm microarrays [29]. In this analysis, the Oncomine database was used to analyze the expression level of CDH13 in different types of cancer.

GEPIA (http://gepia.cancer-pku.cn/index.html) is an interactive online database, developed by Peking University and contains information on tumor and normal tissues from The Cancer Genome Atlas (TCGA) and the Genotype-Tissue Expression project (GTEx) [30]. In this study, the GEPIA database was used to determine the expression level of CDH13 in 33 types of cancer for validating the results from the Oncomine database.

Analysis of the expression of CDH13 at the mRNA level

The RNA sequencing (RNA-seq) data of 533 ccRCC tissues and 72 normal kidney tissues with the corresponding clinicopathological features and survival data were downloaded from The Cancer Genome Atlas (TCGA) database [31]. In this study, we analyzed the expression level of the CDH13 mRNA in ccRCC tissues and normal tissues. We also investigated the level of CDH13 mRNA expression in 72 tumor samples, and 72 paired normal samples based on the TCGA-KIRC dataset.

Gene expression profiles of GSE53757 and GSE40435, obtained from the GPL570 platform (Affymetrix Human Genome U133 Plus 2.0 Array) and GPL10558 (Illumina HumanHT-12 V4.0 Expression Beadchip), were download-

ed from the Gene Expression Omnibus (GEO) database, including 144 and 202 samples, respectively [32, 33]. In this study, the expression level of the CDH13 mRNA in 72 and 101 paired samples from GSE53757 and GSE40435 was analyzed to further verify the results of the expression of the CDH13 mRNA obtained from the TCGA-KIRC dataset.

Analysis of the expression of CDH13 at the protein level

The Clinical Proteomic Tumor Analysis Consortium (CPTAC) (https://proteomics.cancer.gov/programs/cptac), launched in 2011, provides new insights into cancer, based on proteome and proteogenomics [34]. In this study, the CPTAC dataset was used to investigate the expression level of the CDH13 protein in normal and tumor tissues.

The Human Protein Atlas (HPA) (http://www.proteinatlas.org/) is a free online platform that provides protein expression data of 26,941 antibodies targeting 17,165 unique proteins [35]. We used the HPA database to visualize the immunohistochemistry images of CDH13 in ccRCC tissues and normal kidney tissues to verify the results of protein expression obtained from the CPTAC database.

The AlphaFold Protein Structure Database (https://alphafold.ebi.ac.uk/) is an AI system that provides open access to information for predicting the structures of proteins that are a part of the human proteome [36]. We used this database to predict the 3D structure of T-cadherin.

Clinicopathological analysis of CDH13

The University of Alabama Cancer database (UALCAN) (http://ualcan.path.uab.edu/index.html) is a publicly available web resource platform and includes RNA sequence data and clinicopathological data from the TCGA database [37]. We used the UALCAN database to determine the relationship between the expression level of the CDH13 mRNA and clinicopathological features of ccRCC patients. Besides, the association between the CDH13 mRNA expression level and the clinicopathological features of ccRCC patients was further analyzed from the TCGA-KIRC dataset using logistic regression.

The CPTAC database was also used to validate the association of CDH13 and the clinicopathological features in ccRCC patients at the protein level.

Analysis of the diagnostic value of CDH13

Receiver operating characteristic (ROC) curves were plotted to assess the diagnostic performance of CDH13 for diagnosing ccRCC, and the area under curve (AUC) values were calculated to evaluate the validity; AUC values of 0.7-0.9 and > 0.9 are generally considered to indicate good and excellent diagnostic ability, respectively.

Analysis of the prognostic value of CDH13

The Kaplan-Meier survival curves were plotted, and the log-rank test was conducted to estimate the prognostic value of CDH13 in ccRCC patients from the TCGA-KIRC dataset. The primary endpoints of the survival analysis were overall survival (OS) and progression free survival (PFS) in ccRCC patients. Based on the median value of the expression of CDH13, the ccRCC patients were split into the high-expression and low-expression cohorts, respectively. Moreover, the univariate and multivariate analyses were conducted using Cox regression to assess the influence on the survival of ccRCC patients within age, gender, T stage, N stage, M stage, AJCC stage, histology grade, and CDH13 expression to further determine the independent predictors of OS and PFS of ccRCC patients.

Based on the results of the Cox logistic regression analysis, the prognostic predictors were used to construct the nomograms of one-year, three-year, and five-year OS and PFS. The concordance index (C-index) was calculated based on 1,000 bootstrap resamples, and the calibration curves were used to evaluate and visualize the predictive accuracy of the nomogram. All test results were considered to be statistically significant at $P < 0.05$.

Immune infiltration analysis

The Tumor Immune Estimation Resource (TIMER) (https://cistrome.shinyapps.io/timer/) database was initially used to determine the correlation between the expression level of CDH13 and the abundance of six types of

immune cells (B cells, CD8+ T cells, CD4+ T cells, macrophages, neutrophils, and dendritic cells) and six types of immune checkpoints (HAVCR2, CD274, CTLA4, PDCD1, LAG3, and PDCD1LG2) in ccRCC [38]. Then, the Kaplan-Meier plots and the Cox proportional models were used to determine the prognostic value of immune cells and the expression of CDH13 via the survival module in the TIMER database. Finally, using this database, we determined the correlation between the expression level of CDH13 and the levels of gene markers of immune cells.

The ssGSEA was used to quantify the infiltration level of 24 types of immune cells and determine the correlation between the expression level of CDH13 and immune infiltration [39, 40]. The Wilcoxon rank sum test was conducted to evaluate the difference in immune cells between the CDH13-high and CDH13-low cohorts.

The Tumor and Immune System Interaction Database (TISIDB) (http://cis.hku.hk/TISIDB/) was used to perform Spearman's correlation analysis between the expression of CDH13 and tumor lymphocyte infiltration, immunoinhibitors, immunostimulators, and the major histocompatibility complex [41].

Analysis of the methylation of CDH13

Initially, we evaluated the expression levels of 23 types of m6A regulators in tumor and normal tissues, including seven writers (METTL3, METTL14, RBM15B, RBM15, VIRMA, WTAP, CBLL1, and ZC3H13), two erasers (FTO and ALKBH5), and 11 readers (YTHDF1, YTHDF2, YTHDF3, YTHDC1, YTHDC2, HNRNPC, HNRNPA2B1, IGF2BP1, IGF2BP2, IGF2BP3, LRPPRC, FMR1, and ELAVL1) based on the TCGA-KIRC dataset. Then, we performed a correlation analysis of CDH13 and 23 m6A regulators. Next, we calculated the risk scores based on the parameters selected from CDH13 and 23 m6A regulators using the LASSO regression. Subsequently, the patients were classified into high-risk and low-risk groups by the median risk score value, and the survival analysis was performed to assess the prognostic value. The ROC curves were also used for analyzing the sensitivity and specificity and evaluating the accuracy of the models.

The TCGA-KIRC Methylation 450 K data were downloaded from UCSC Xena (http://xena.ucsc.edu/) [42]. We obtained CDH13 promoter methylation data of 319 ccRCC patients with survival data. And the data were used for conducting expression, correlation, and survival analyses. The intersection was determined between differentially expressed regions, negatively correlated regions, and significantly prognostic regions by plotting a Venn diagram to determine the core methylation regions of CDH13.

Genetic alteration analysis

The cBio Cancer Genomics Portal (cBioPortal) (http://www.cbioportal.org/) is an open-access platform for the interactive exploration of multiple cancer genomics data [43]. Based on the TCGA-KIRC dataset, the cBioPortal database was used to comprehensively analyze and visualize genetic mutations, putative copy-number alterations, and mRNA expression using a z-score threshold of ±2.0 (RNA Seq V2 RSEM). We also constructed Kaplan-Meier plots to assess the prognostic value of the genetic alteration of CDH13 in ccRCC patients.

Protein-protein interaction (PPI) network analysis

The Search Tool for the Retrieval of Interacting Genes/Proteins (STRING) (https://string-db.org/) is an online analytical platform for constructing and visualizing protein-protein interaction networks [44]. We built a PPI network of CDH13 for predicting its functional partners.

Metascape (https://metascape.org/) is a comprehensive analysis web resource for gene annotation and enrichment analysis [45]. We used this database to validate the protein-protein interaction network and investigate the Molecular Complex Detection (MCODE) components by identifying CDH13 and its correlated genes.

Functional enrichment analysis

We performed the Gene Ontology (GO) analysis and the Kyoto Encyclopedia of Genes and Genomes (KEGG) pathway analysis of CDH13 and its correlated genes to elucidate the potential functions of CDH13 in ccRCC.

Quantitative reverse transcriptase polymerase chain reaction (qRT-PCR)

The ethics committee of the First Hospital of Shanxi Medical University approved the use of human tissues for detecting the expression level of CDH13 in normal kidney tissues and ccRCC tissues in this study. All samples were collected from the Department of Urology, First Hospital of Shanxi Medical University, after radical nephrectomy. The pathological examination was performed by the Department of Pathology, First Hospital of Shanxi Medical University. We obtained written informed consent from all patients.

Total RNA from clinical tissue samples was extracted using TransZol Up (TransGen Biotech, China), and cDNA was synthesized by reverse transcription (TransGen Biotech, China) following the manufacturer's instructions. We performed qRT-PCR using Roche Lightcycler 96, following the protocols of the manufacturer, and GAPDH was used as an endogenous control for normalization. The primer sequences for CDH13 and GAPDH are provided in Table S1.

Western blot assay

Proteins were isolated from clinical tissue samples using the RIPA buffer (Boster, China), and the concentration of total protein was quantitated using a BCA kit (Boster, China). Then, the protein samples were separated using SDS-PAGE gels (Meilunbio, China) and transferred onto PVDF membranes (Boster, China). After blocking using 10% skimmed milk powder, the membranes were incubated overnight at 4°C with the anti-CDH13 antibody (1:1000; Abcam, USA) or the anti-GAPDH antibody (1:1000; Boster, China). After washing thrice with TBST, the membranes were incubated with a secondary antibody (1:2000, Boster, China) at room temperature for 2 h. Finally, the signal was visualized using an enhanced chemiluminescence kit (Boster, China) and analyzed using the Image J software.

Immunohistochemistry (IHC)

The tissues were initially embedded in paraffin. Then they were cut into sections, deparaffinized, and hydrated. Following antigen retrieval, the samples were blocked by endogenous peroxidases. The slides were immunostained using anti-CDH13 antibodies (1:100, ABclonal Technology, China) and a secondary antibody (ZSGB-BIO, China). Then, the histological sections were stained with DAB and counterstained with hematoxylin to detect the protein expression level of CDH13. Next, the Image-Pro Plus software (version 6.0) was used to analyze the immunohistochemistry images, and the integral optical density (IOD)/Area was evaluated to quantify the expression level of CDH13.

Statistical analysis

We conducted Student's t-tests and paired Student's t-tests to compare the differences between groups. Kruskal-Wallis H-test and Dunn's test were conducted to evaluate the relationships between the clinicopathological features and the expression of CDH13. The hazard ratios (HRs) with 95% confidence intervals (CIs) from Kaplan-Meier curves and the *P*-values from log-rank tests were used for the survival analysis. The univariate and multivariate Cox regression analyses were performed to identify the independent prognostic predictors. Pearson's and Spearman's correlation tests were conducted to determine the correlation. The statistical analysis was conducted using SPSS 26.0 and the R software (version 3.6.1). The figures were constructed using the R software (version 3.6.1) and the corresponding online databases. The results of all tests were considered to be statistically significant at $P < 0.05$. The flow diagram of this study is presented in **Figure 1**.

Results

The expression level of CDH13 in patients with different types of cancer

Initially, the expression level of the CDH13 mRNA was compared between 20 common cancer tissues and the corresponding normal tissues using the Oncomine database. The transcriptional expression of CDH13 was considerably lower in normal kidney tissues than in cancer tissues (**Figure 2A**). We also used the GEPIA database to further analyze the expression level of CDH13 in 33 types of cancer, including ccRCC. The expression of the CDH13 mRNA was considerably higher in the cancer tissues than in the normal kidney tissues, which was similar to the results obtained from the Oncomine database (**Figure 2B**).

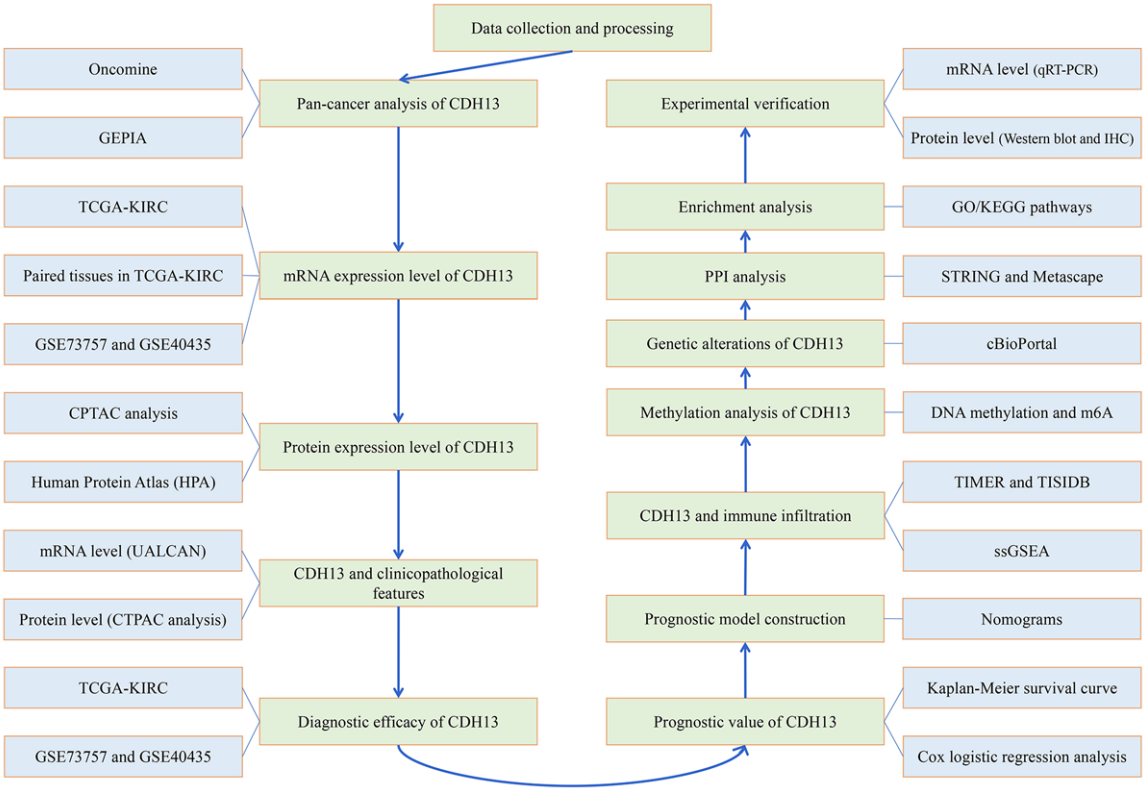

Figure 1. The flowchart of this study.

The expression level of the CDH13 mRNA in ccRCC patients

In this analysis, we measured the expression level of the CDH13 mRNA based on the TCGA-KIRC dataset. The results suggested that the expression of the CDH13 mRNA was significantly higher in ccRCC tissues compared to that in the normal tissues (**Figure 3A**, **3B**). The analysis of the expression of the CDH13 mRNA from GSE53757 and GSE40435 indicated similar overexpression patterns in the ccRCC samples compared to that in the normal tissues (**Figure 3C**, **3D**). These results further validated the findings of the analysis performed using the TCGA-KIRC dataset.

The expression level of the CDH13 protein in patients with ccRCC

Besides analyzing the expression of the CDH13 mRNA, we also analyzed the expression of CDH13 at the protein level using the CPTAC database and the HPA database. The protein level of CDH13 in 84 normal tissues was significantly lower than that in 110 ccRCC samples from the CPTAC database ($P < 0.001$) (**Figure 3E**). A higher level of expression of the CDH13 protein was also found in the ccRCC tissues than that in the normal tissues, as visualized by the representative immunohistochemical images from the HPA database (**Figure 3F**). The 3D structure of T-cadherin predicted by the AlphaFold database is shown in **Figure 3G**.

To summarize, these results indicated that CDH13 is upregulated in ccRCC at the transcriptional and translational levels.

Relationship between the expression level of CDH13 and the clinicopathological features of ccRCC patients

To determine the relationship between the expression of the CDH13 mRNA and the clinicopathological features of ccRCC patients, the characteristics of the ccRCC patients from the TCGA-KIRC dataset were analyzed (Figure S1). The level of expression of the CDH13 mRNA was significantly correlated with the T stage, M stage, AJCC stage, and histologic grade (**Table 1**). Based on the UALCAN database, CDH13 was found to be strongly associated with the ccRCC stages and tumor grades at the mRNA level (Figure S2 and Table S2). The results of

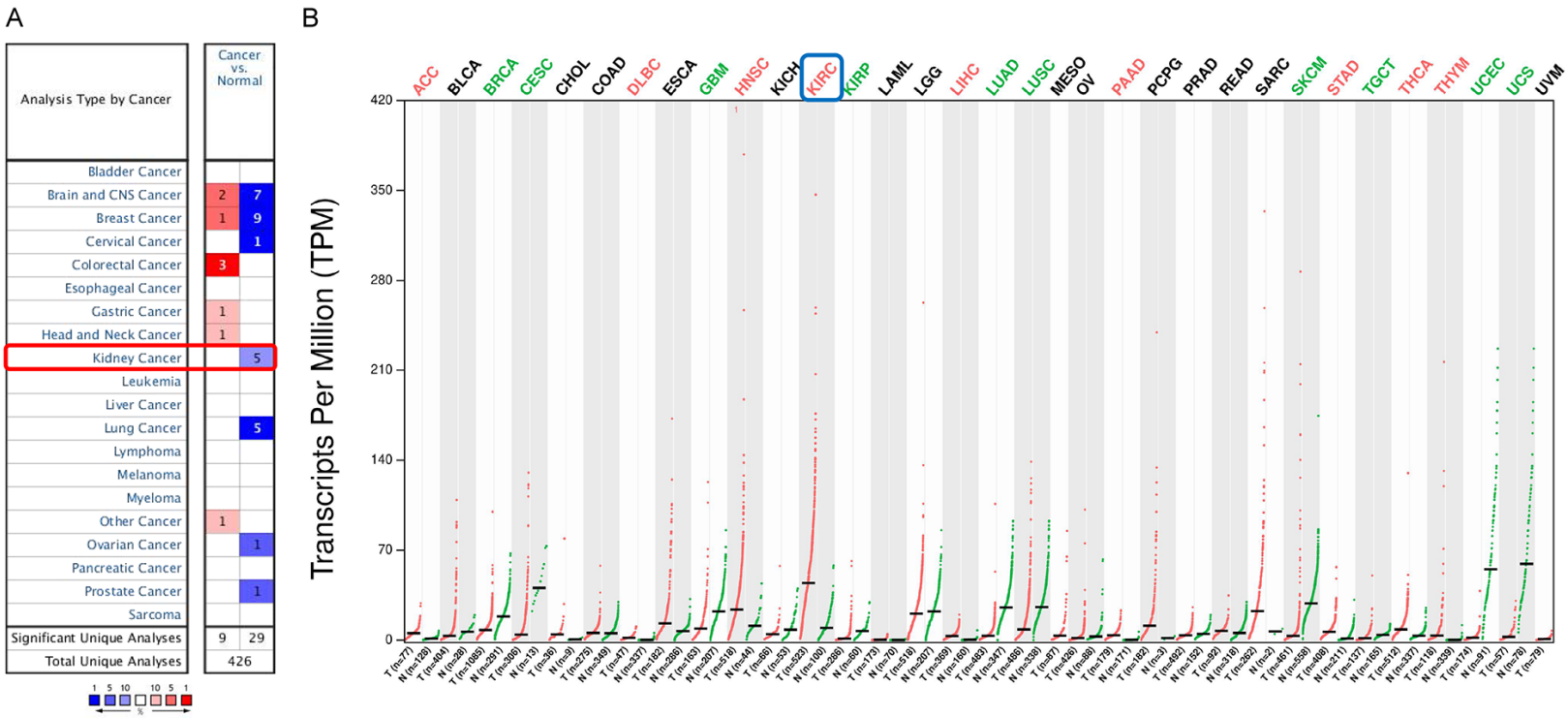

Figure 2. The expression level of CDH13 in different types of tumor tissues and normal tissues. A. Oncomine. B. GEPIA.

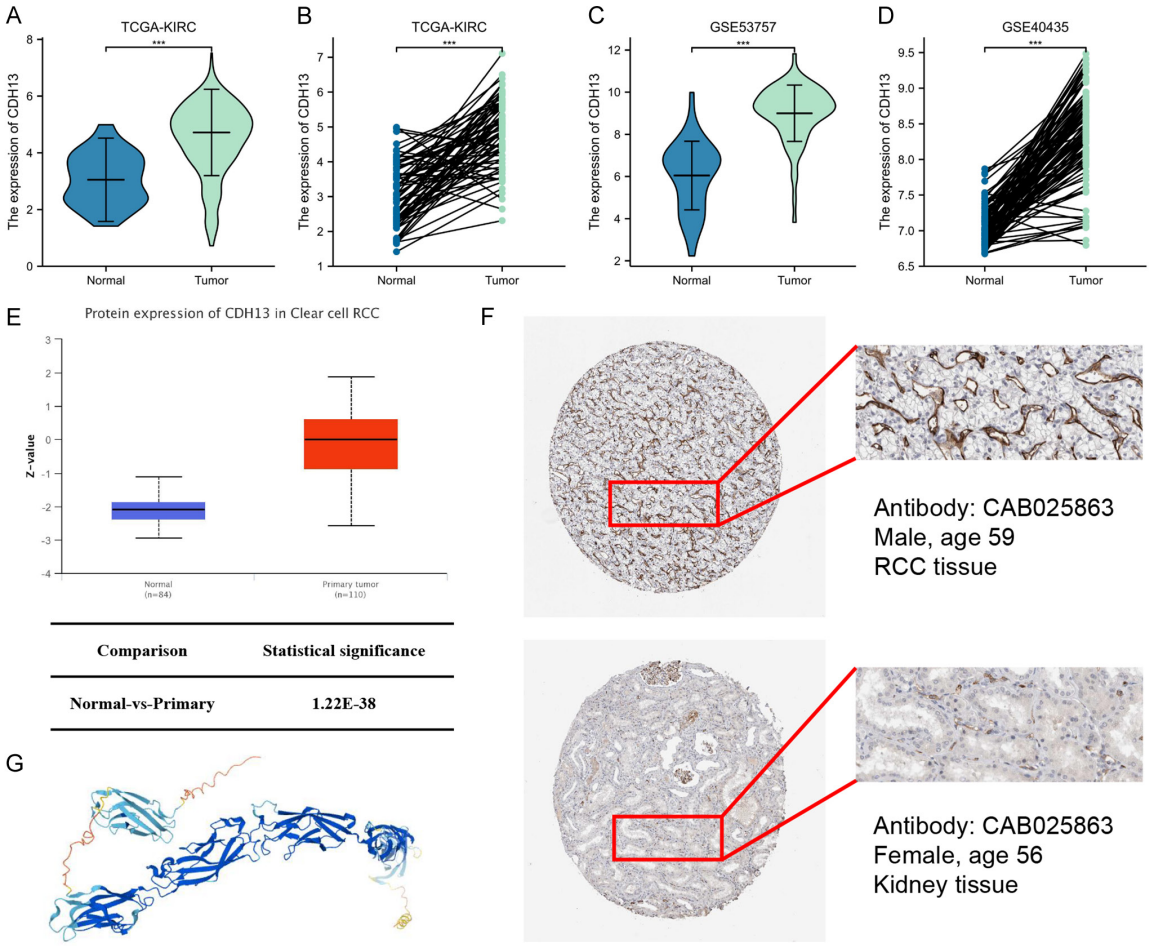

Figure 3. The mRNA and protein expression level of CDH13 in ccRCC patients. A. CDH13 mRNA expression between normal tissues (n=72) and tumor tissues (n=539) from TCGA-KIRC dataset. B. CDH13 mRNA expression between normal tissues (n=72) and matched tumor tissues (n=72) from TCGA-KIRC dataset. C. CDH13 mRNA expression between normal tissues (n=72) and matched tumor tissues (n=72) from GEO dataset (GSE53757). D. CDH13 mRNA expression between normal tissues (n=72) and matched tumor tissues (n=72) from GEO dataset (GSE40435). E. CDH13 protein expression between normal tissues (n=84) and tumor tissues (n=110) from CPTAC dataset. F. Immunohistochemical staining of CDH13 expression in ccRCC tissue and normal tissue from Human Protein Atlas (HPA). G. 3D structure of Cadherin-13 (Alphafold) (***P < 0.001).

the logistic regression analysis indicated that the expression level of the CDH13 mRNA was positively correlated with the T stage, M stage, AJCC stage, and histology grade (**Table 2**). The results from the CPTAC database showed that the expression level of the CDH13 protein was also closely related to the cancer stages and tumor grades (Figure S2 and Table S2). Similar to the results from the UALCAN database, the ccRCC patients with Stage 1 and Grade 1 were found to have the highest level of CDH13 protein expression. The results also indicated that the expression of CDH13 did not differ significantly with gender and age in ccRCC patients at the mRNA and protein levels (Figure S2 and Table S2).

To summarize, these results showed that CDH13 might be associated with tumor development and progression in ccRCC patients.

The diagnostic efficacy of CDH13 in the diagnosis of ccRCC

In this analysis, the ROC curves and AUC values were used to evaluate the diagnostic performance of CDH13 for diagnosing ccRCC. Based on the ROC analysis of the data on the ccRCC patients from the TCGA-KIRC dataset, the AUC value of CDH13 was 0.822 (95% CI: 0.784-0.861), which indicated that CDH13 had a good diagnostic ability (**Figure 4A**). Based on the ROC analysis of the data on the ccRCC patients

Table 1. The association between the mRNA expression of CDH13 and the clinicopathological features of ccRCC patients from TCGA-KIRC dataset

Clinicopathological features	Low expression of CDH13	High expression of CDH13	*p* value
N	269	270	
Age, mean ± SD	60.94±11.93	60.32±12.27	0.553
Gender, n (%)			0.252
Female	86 (16%)	100 (18.6%)	
Male	183 (34%)	170 (31.5%)	
T stage, n (%)			0.003
T1	118 (21.9%)	160 (29.7%)	
T2	42 (7.8%)	29 (5.4%)	
T3	101 (18.7%)	78 (14.5%)	
T4	8 (1.5%)	3 (0.6%)	
N stage, n (%)			0.110
N0	123 (47.9%)	118 (45.9%)	
N1	12 (4.7%)	4 (1.6%)	
M stage, n (%)			0.002
M0	201 (39.7%)	227 (44.9%)	
M1	52 (10.3%)	26 (5.1%)	
AJCC stage, n (%)			< 0.001
Stage I	114 (21.3%)	158 (29.5%)	
Stage II	33 (6.2%)	26 (4.9%)	
Stage III	67 (12.5%)	56 (10.4%)	
Stage IV	54 (10.1%)	28 (5.2%)	
Histologic grade, n (%)			< 0.001
G1	5 (0.9%)	9 (1.7%)	
G2	90 (16.9%)	145 (27.3%)	
G3	116 (21.8%)	91 (17.1%)	
G4	52 (9.8%)	23 (4.3%)	
Laterality, n (%)			0.391
Left	131 (24.3%)	121 (22.5%)	
Right	137 (25.5%)	149 (27.7%)	
OS event, n (%)			< 0.001
Alive	158 (29.3%)	208 (38.6%)	
Dead	111 (20.6%)	62 (11.5%)	
PFS event, n (%)			0.004
Alive	173 (32.1%)	205 (38%)	
Dead	96 (17.8%)	65 (12.1%)	

from GSE53757 and GSE40435, the AUC value was 0.923 (95% CI: 0.875-0.972) and 0.956 (95% CI: 0.927-0.985), respectively, which indicated an excellent diagnostic ability of CDH13 (**Figure 4B**, **4C**). These results were similar to those obtained by analyzing the data from the TCGA-KIRC dataset.

The results of the ROC analysis thus indicated the diagnostic value of CDH13 in ccRCC.

The prognostic value of CDH13 in ccRCC patients

To determine the prognostic value of CDH13 in ccRCC patients, the Kaplan-Meier survival curves were plotted and log-rank tests were conducted initially to perform the survival analysis based on the data from TCGA-KIRC. The results showed that the elevated expression level of the CDH13 mRNA was significantly correlated with higher OS (HR: 0.53, 95% CI: 0.39-0.72, P < 0.001) and higher PFS (HR: 0.65, 95% CI: 0.47-0.89, *P*=0.007) (**Figure 5A**, **5B**).

To further validate these results, we constructed Cox regression models by performing univariate and multivariate analyses. The results of the univariate Cox regression analysis indicated that the pT stage, pN stage, pM stage, AJCC stage, histology grade, and CDH13 were closely related to OS and PFS of ccRCC patients (**Tables 3** and **4**). The results of the multivariate Cox regression analysis showed that the CDH13 expression level was an independent predictor of OS and PFS of ccRCC patients. Based on these results of Cox logistic regression analyses, the prognostic predictors were used to construct the nomograms of one-year, three-year, and five-year OS and PFS. These nomograms were used to quantitatively predict the prognosis of ccRCC patients (**Figure 5C**, **5D**). The C-indices of the predicted OS and PFS were 0.757 (0.732-0.783) and 0.806 (0.782-0.830), respectively. The calibration plots showed good consistency between the prediction and observation of OS and PFS (**Figure 5E**, **5F**).

To summarize, CDH13 might be a prognostic biomarker for predicting the prognosis of ccRCC patients.

Correlation between CDH13 and immune infiltration in ccRCC patients

We used the TIMER database, ssGSEA, and the TISIDB database to analyze the correlation between the CDH13 expression level and immune

Table 2. The association between CDH13 expression and clinicopathological features in the ccRCC patients from TCGA-KIRC dataset based on logistic regression

Clinicopathological features	OR	95% CI	*p* value
Age (< 65 *vs* ≥ 65)	1.007	0.719-1.412	0.966
Gender (Male *vs* Female)	0.799	0.559-1.140	0.216
Laterality (Right *vs* Left)	1.177	0.839-1.654	0.345
T stage (T1-T2 *vs* T3-T4)	1.590	1.114-2.274	0.011
N stage (N0 *vs* N1)	2.878	0.972-10.522	0.074
M stage (M0 *vs* M1)	2.259	1.372-3.800	0.002
AJCC stage (I-II *vs* III-IV)	1.803	1.269-2.571	0.001
Histologic grade (G1-G2 *vs* G3-G4)	2.389	1.688-3.396	< 0.001

infiltration in ccRCC. The results based on the TIMER database indicated that CDH13 was strongly correlated with the infiltration of CD8+ T cells, CD4+ T cells, macrophages, neutrophils, and dendritic cells (Figure S3A). Additionally, the expression level of CDH13 showed a significantly positive correlation with five types of immune checkpoints in ccRCC, including PDCD1, CD274, PDCD1LG2, CTLA4, and LAG3 (Figure S3B). Additionally, the Kaplan-Meier plots constructed using the TIMER database indicated that the infiltration of six types of immune cells was not correlated with the OS of the ccRCC patients (Figure S3C). The Cox proportional hazard model showed that macrophages, neutrophils, and CDH13 expression levels were the prognostic biomarkers in the ccRCC patients (Table S3). The TIMER database was used to evaluate the correlation between the CDH13 expression and the level of gene markers for immune cells. The expression of CDH13 was significantly correlated with the abundance of gene markers for immune cells (Table S4).

The results based on the ssGSEA showed that the expression level of CDH13 in most immune cells differed between the CDH13-high and CDH13-low cohorts (Figure S4A). Additionally, the expression level of CDH13 was correlated with the enrichment of CD56bright NK cells, mast cells, NK cells, and pDC (Figure S4B and S4C).

The TISIDB database was used to perform Spearman's correlation between the CDH13 expression level and tumor lymphocyte, immunoinhibitors, immunostimulators, and the major histocompatibility complex. The results of this analysis indicated that the expression level of CDH13 was significantly correlated with some immunoinhibitors, especially KDR, immunostimulators, especially ENTPD1, and the major histocompatibility complex, especially HLA-E (Figure S5 and Tables S5, S6, S7, S8).

To summarize, these results confirmed that CDH13 strongly affects the immune infiltration in ccRCC.

Methylation analysis of CDH13

We investigated the expression levels of 23 m6A regulators. The expression levels of writers, erasers, and readers differed considerably between normal kidney tissues and ccRCC tissues (**Figure 6A-C**). The results of the correlation analysis suggested that the expression level of CDH13 was significantly correlated with the expression levels of METTL14, RBM15B, VIRMA, ZC3H13, FTO, YTHDF2, YTHDC1, and HNRNPC (**Figure 6D**). We also performed a LASSO regression analysis with 10-fold cross-validation to identify the prognostic factors that were significantly correlated with the prognosis of ccRCC patients based on CDH13 and 23 m6A regulators (**Figure 6E**, **6F**). We constructed the prognostic model and calculated the risk scores for each ccRCC patient based on 11 genes (**Figure 6G**, **6H**). The results of the survival analysis indicated that the patients in high-risk groups had worse OS (**Figure 6I**). The AUC value calculated based on the ROC curve was high, which indicated the prognostic accuracy of the model (**Figure 6J**).

We also analyzed the methylation of CpG islands in the promoter regions of CDH13 using the DNA methylation data from 319 ccRCC patients in the TCGA-KIRC dataset. The results showed that most of the CpG islands (29/50) were significantly hypermethylated in normal tissues (**Figure 7A**). The correlation analysis indicated that the methylation status of 22 regions was negatively associated with the expression of the CDH13 mRNA (**Figure 7B**) and the survival analysis showed that the level of methylation of 15 CpG islands was correlated with OS of the ccRCC patients (**Figure 7C**). The results showed that cg03474070 was the core methylation region of CDH13 (**Figure 7D**).

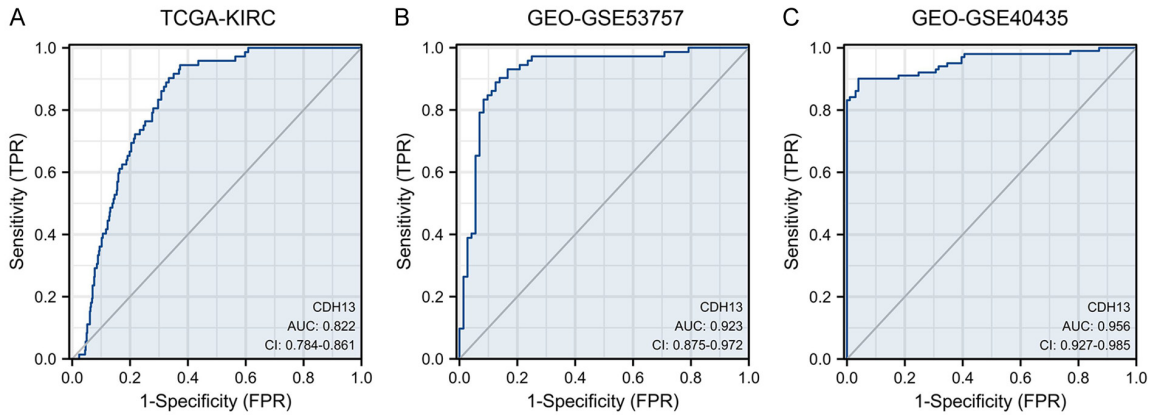

Figure 4. ROC curves of CDH13 for diagnosing ccRCC. A. TCGA-KIRC dataset. B. GEO-GSE53757. C. GEO-GSE40435.

These results highlighted the epigenetic patterns of CDH13 and the association between the methylation of CDH13 and the prognosis of ccRCC patients.

Genetic alterations of CDH13 in patients with ccRCC

The cBioPortal database was used to determine the genetic alteration rate of CDH13 in ccRCC and further analyze their correlation with the clinical outcome of ccRCC patients. The rate of genetic alteration in CDH13 was found to be 4% based on the analysis of the data of 512 ccRCC patients from the TCGA-KIRC dataset (**Figure 8A**). The types of mutations included amplification, deep deletion, mRNA high, and missense mutation. The results of the Kaplan-Meier plots indicated that the OS and DSS of the ccRCC patients without CDH13 mutations were significantly worse (**Figure 8B**, **8C**).

The cBioPortal online tool was also used to analyze the well-recognized hypermutated genes, including VHL, PBRM1, SETD2, BAP1, and MTOR, in the ccRCC patients. The results showed that the alteration rate of VHL differed between the CDH13-high and CDH13-low cohorts (Figure S6). This difference was also observed in the PBRM1, SETD2, BAP1, and MTOR genes (Figure S6).

These results indicated that the clinical outcome of the ccRCC patients was affected by the expression and the genetic mutations of CDH13.

Protein-protein interaction network of CDH13

The correlation analysis showed the top 25 genes that were positively and negatively correlated with CDH13 in ccRCC (Figure S7A). The correlation circle showed the correlation between the expression level of CDH13 and the expression of the top 10 positively and negatively correlated genes (Figure S7B). Next, we built a PPI network of CDH13 and predicted the functional partners of CDH13 using the STRING and Metascape databases. The results from the STRING database showed that the top 10 proteins were catenin beta-1 (CTNNB1), catenin delta-1 (CTNND1), junction plakoglobin (JUP), catenin alpha-1 (CTNNA1), cadherin-11 (CDH11), cadherin-17 (CDH17), cadherin-8 (CDH8), cadherin-9 (CDH9), cadherin-10 (CDH10), and cadherin-5 (CDH5) (**Figure 9**). The results from the Metascape database also revealed the PPI network and the MCODE components identified in CDH13 and its correlated genes. The biological function was closely associated with focal adhesion, the PI3K/Akt signaling pathway (MCODE 1), the Notch signaling pathway, positive regulation of the Notch signaling pathway (MCODE 2), activin binding, type I transforming growth factor beta receptor binding, and the activity of the transforming growth factor beta-activated receptor (MCODE 3) (Figure S8).

GO and KEGG enrichment analyses of CDH13

The results of the GO and KEGG enrichment analyses of CDH13 and its correlated genes showed that in ccRCC, CDH13 was mainly

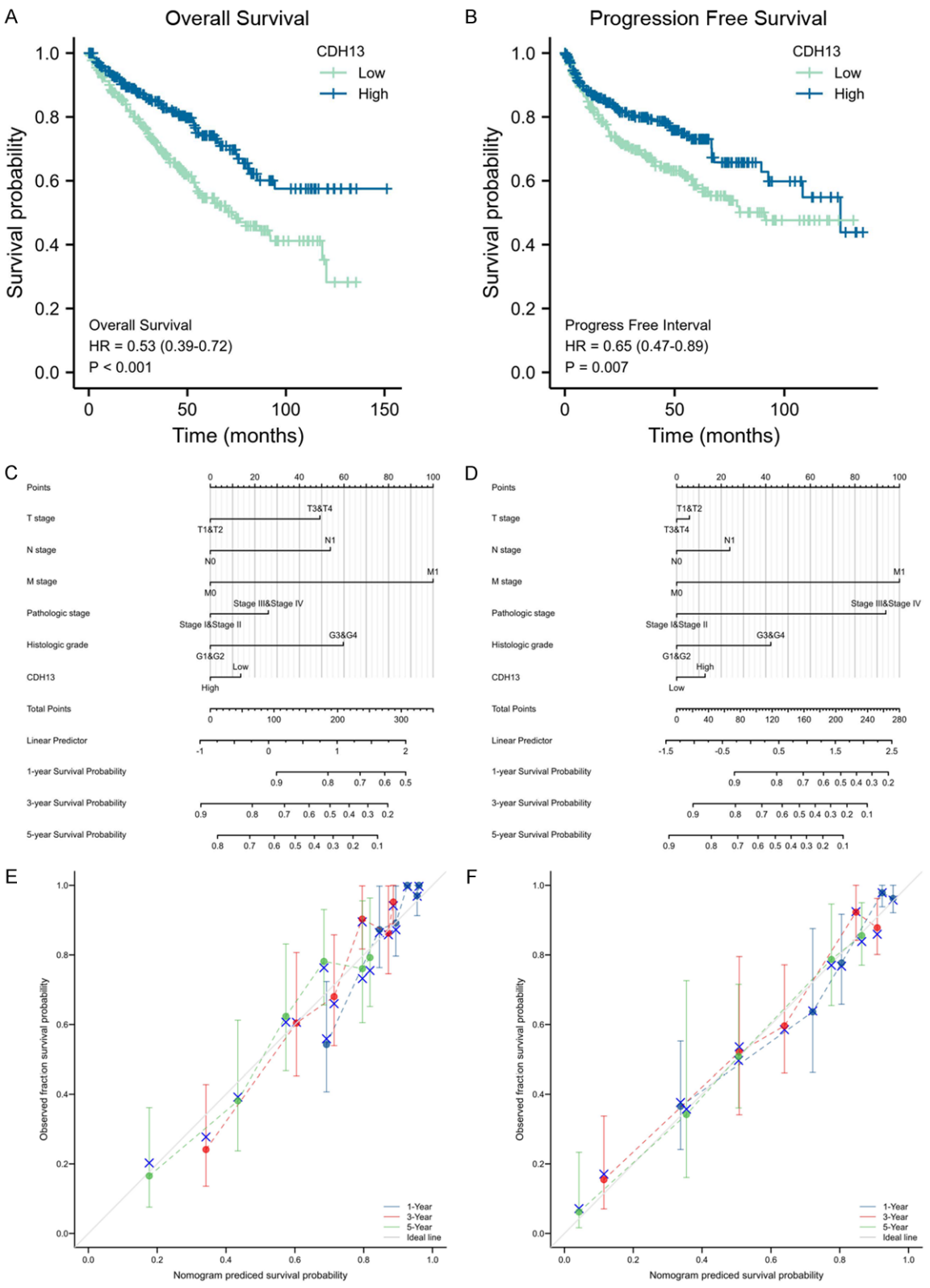

Figure 5. The survival analysis of CDH13 in ccRCC patients from TCGA-KIRC dataset. A. The Kaplan-Meier survival curve comparing the high and low expression of CDH13 in overall survival (OS). B. The Kaplan-Meier survival curve comparing the high and low expression of CDH13 in progression free survival (PFS). C. Nomogram for the prediction of OS in ccRCC patients. D. Nomogram for the prediction of PFS in ccRCC patients. E. Calibration plot of the nomogram for prediction of OS in ccRCC patients. F. Calibration plot of the nomogram for prediction of PFS in ccRCC patients.

Table 3. Univariate and multivariate cox logistic regression analysis of OS in ccRCC patients based on TCGA-KIRC cohort

Clinicopathological features	Univariate analysis			Multivariate analysis		
	HR	95% CI	*p* value	HR	95% CI	*p* value
Age						
Age ≥ 65 *vs* Age < 65	1.363	0.906-2.051	0.137	1.534	0.996-2.363	0.052
Gender						
Male *vs* Female	1.059	0.698-1.609	0.787	1.105	0.717-1.704	0.651
pT stage						
T3-T4 *vs* T1-T2	3.061	2.016-4.647	< 0.001	1.506	0.662-3.428	0.329
pN stage						
N1 *vs* N0	3.064	1.582-5.934	0.001	1.495	0.747-2.992	0.256
pM stage						
M1 *vs* M0	4.188	2.721-6.448	0.001	2.769	1.638-4.678	< 0.001
AJCC stage						
III-IV *vs* I-II	3.472	2.243-5.373	< 0.001	1.224	0.475-3.152	0.676
Histology grade						
G3-G4 *vs* G1-G2	2.612	1.651-4.138	< 0.001	1.629	0.997-2.662	0.052
CDH13						
High *vs* Low	0.404	0.259-0.631	< 0.001	0.529	0.333-0.841	0.007

Table 4. Univariate and multivariate cox logistic regression analysis of PFS in ccRCC patients based on TCGA-KIRC cohort

Clinicopathological features	Univariate analysis			Multivariate analysis		
	HR	95% CI	*p* value	HR	95% CI	*p* value
Age						
Age ≥ 65 *vs* Age < 65	0.862	0.553-1.343	0.511	0.987	0.609-1.599	0.957
Gender						
Male *vs* Female	1.178	0.760-1.824	0.464	1.271	0.794-2.034	0.317
pT stage						
T3-T4 *vs* T1-T2	4.122	2.638-6.441	< 0.001	1.007	0.497-2.039	0.984
pN stage						
N1 *vs* N0	3.604	1.851-7.017	< 0.001	1.256	0.631-2.500	0.516
pM stage						
M1 *vs* M0	8.847	5.667-13.814	< 0.001	4.232	2.513-7.126	< 0.001
AJCC stage						
III-IV *vs* I-II	6.734	4.030-11.251	< 0.001	3.484	1.434-8.461	0.006
Histology grade						
G3-G4 *vs* G1-G2	2.747	1.702-4.434	< 0.001	1.742	1.043-2.909	0.034
CDH13						
High *vs* Low	0.399	0.192-0.833	0.014	0.792	0.646-0.971	0.025

enriched in the development of the glomerulus (Biological process), membrane microdomain (Cellular component), transmembrane receptor protein kinase activity (Molecular function), and the Ras signaling pathway (KEGG pathway) (**Figure 10**).

The qRT-PCR, Western blot assay, and IHC

To confirm the mRNA expression level of CDH13, we conducted qRT-PCR in 40 paired ccRCC tissues and adjacent normal kidney tissues. The results showed that the CDH13

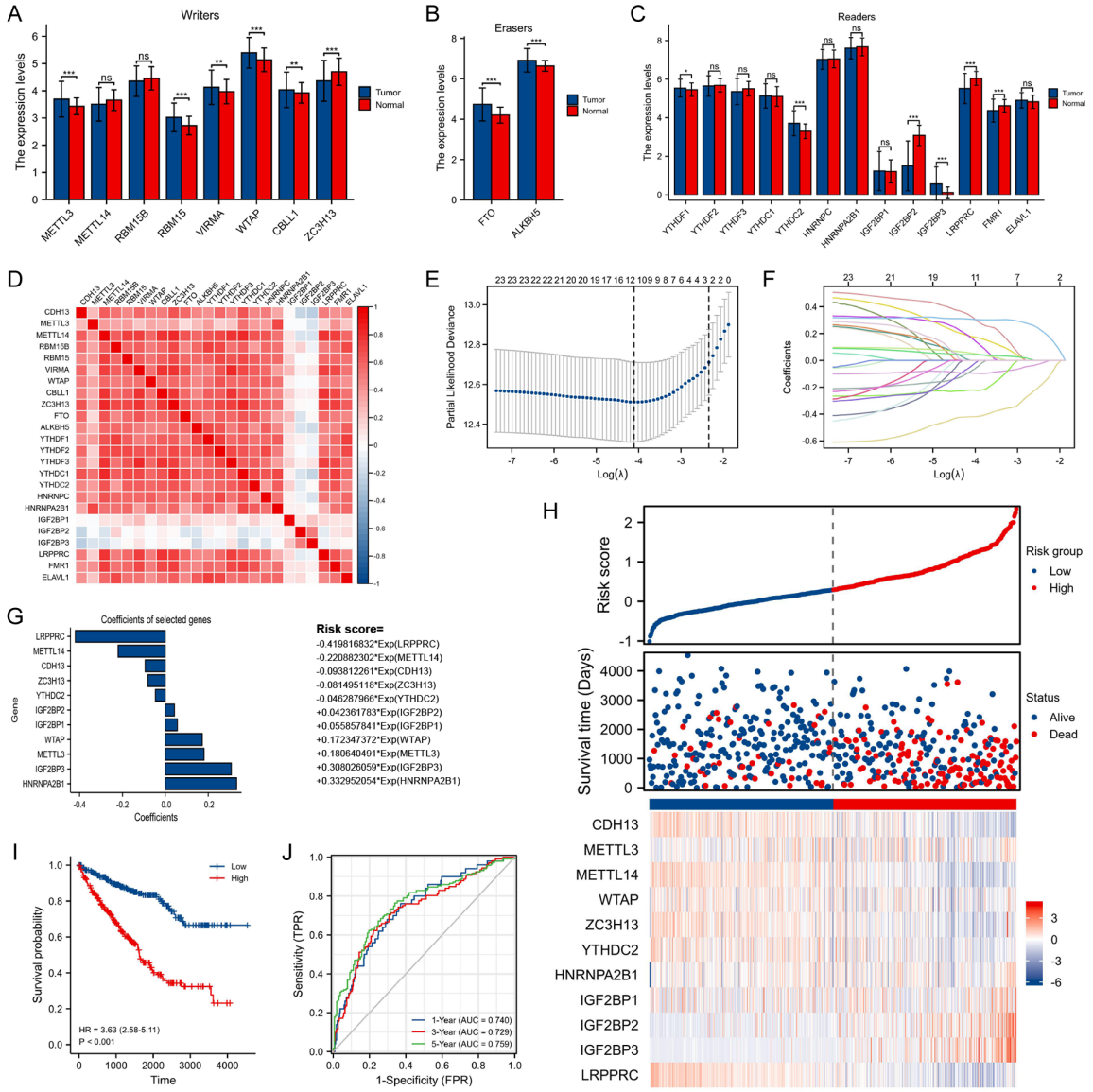

Figure 6. A. The expression levels of seven writers in the tumor tissues and normal tissues. B. The expression levels of two erasers in the tumor tissues and normal tissues. C. The expression levels of eleven readers in the tumor tissues and normal tissues. D. Correlation heatmap of CDH13 and 23 m6A regulators in ccRCC. E, F. LASSO coefficients profiles of CDH13 and 23 m6A regulators and LASSO regression with 10 fold cross-validation obtained eleven prognostic genes using minimum lambda value. G. Coefficients of selected genes and the risk score formula. H. The distribution of the risk score and the survival status of each patient. I. The Kaplan-Meier curve of the ccRCC patients in high-risk and low-risk groups (OS). J. The ROC curve of the prognostic model (***P < 0.001, **P < 0.01, *P < 0.05).

mRNA expression was significantly higher in the ccRCC tissues than in the normal kidney tissues (**Figure 11A**). The results of the Western blot assays were also similar, indicating that the expression of the CDH13 protein was upregulated in the ccRCC tissues (**Figure 11B**). Moreover, immunohistochemical staining was performed to determine the expression level of CDH13 in the low-grade ccRCC tissues, the high-grade ccRCC tissues, and normal kidney tissues. The expression level of CDH13 was significantly lower in the normal kidney tissues than that in the ccRCC tissues (**Figure 11C**, **11D**). The expression level of CDH13 was considerably higher in the low-grade ccRCC tissues than that in the high-grade ccRCC tissues. These results based on immunohistochemical staining confirmed the expression patterns of

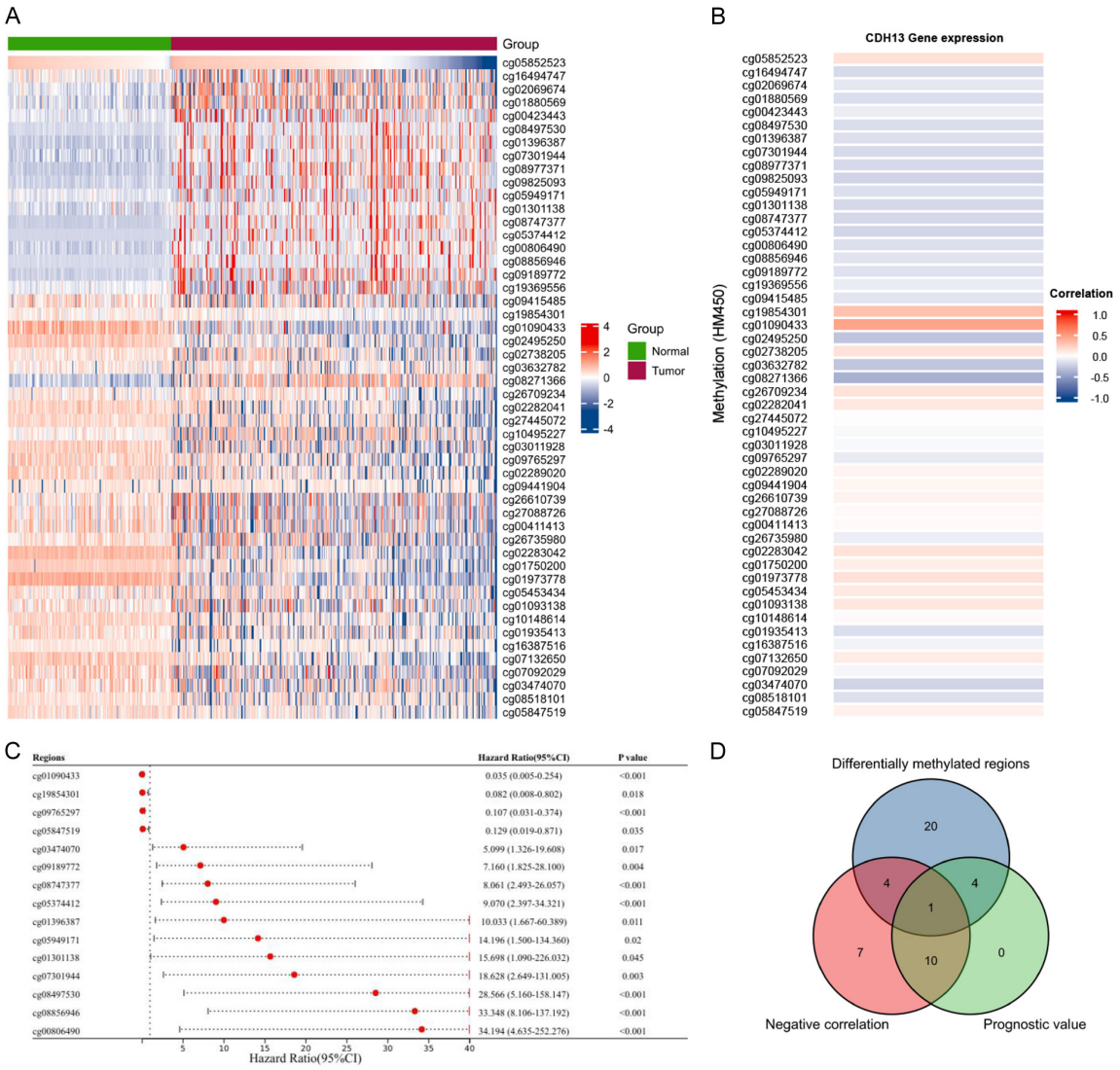

Figure 7. A. Heatmap of the methylation levels of CpG sites of CDH13 in TCGA-KIRC. B. Correlation heatmap of the CDH13 mRNA expression and the methylation status of CpG regions in TCGA-KIRC. C. Forrest plot of survival analysis of CpG islands. D. Venn diagram identifying the core methylation regions of CDH13.

CDH13 that were determined using the other databases.

Discussion

CDH13 is an atypical member of the cadherin family and strongly influences the maintenance of cell structure, regulation of cell growth, angiogenesis, cell recognition, cell adhesion, and intercellular signaling [19, 20, 22]. In this study, we comprehensively investigated the level of expression, diagnostic efficacy, prognostic value, immune infiltration, methylation status, genetic alteration, and function enrichment of CDH13 in ccRCC patients. It has been demonstrated by previous studies that the expression level of CDH13 was found to decrease in various malignancies, such as pancreatic cancer [28], colorectal adenocarcinoma [46], prostate cancer [47], and lung cancer [48]. In this study, we found that the expression level of CDH13 increased at the mRNA and protein levels in ccRCC patients, which was different from the level of expression of CDH13 in other types of cancer, suggesting a distinctive expression pattern in patients with ccRCC. The analysis of the clinical samples showed that the expression of the CDH13 mRNA increased significantly in the ccRCC tissues relative to that in matched normal tissues. Similarly, the results

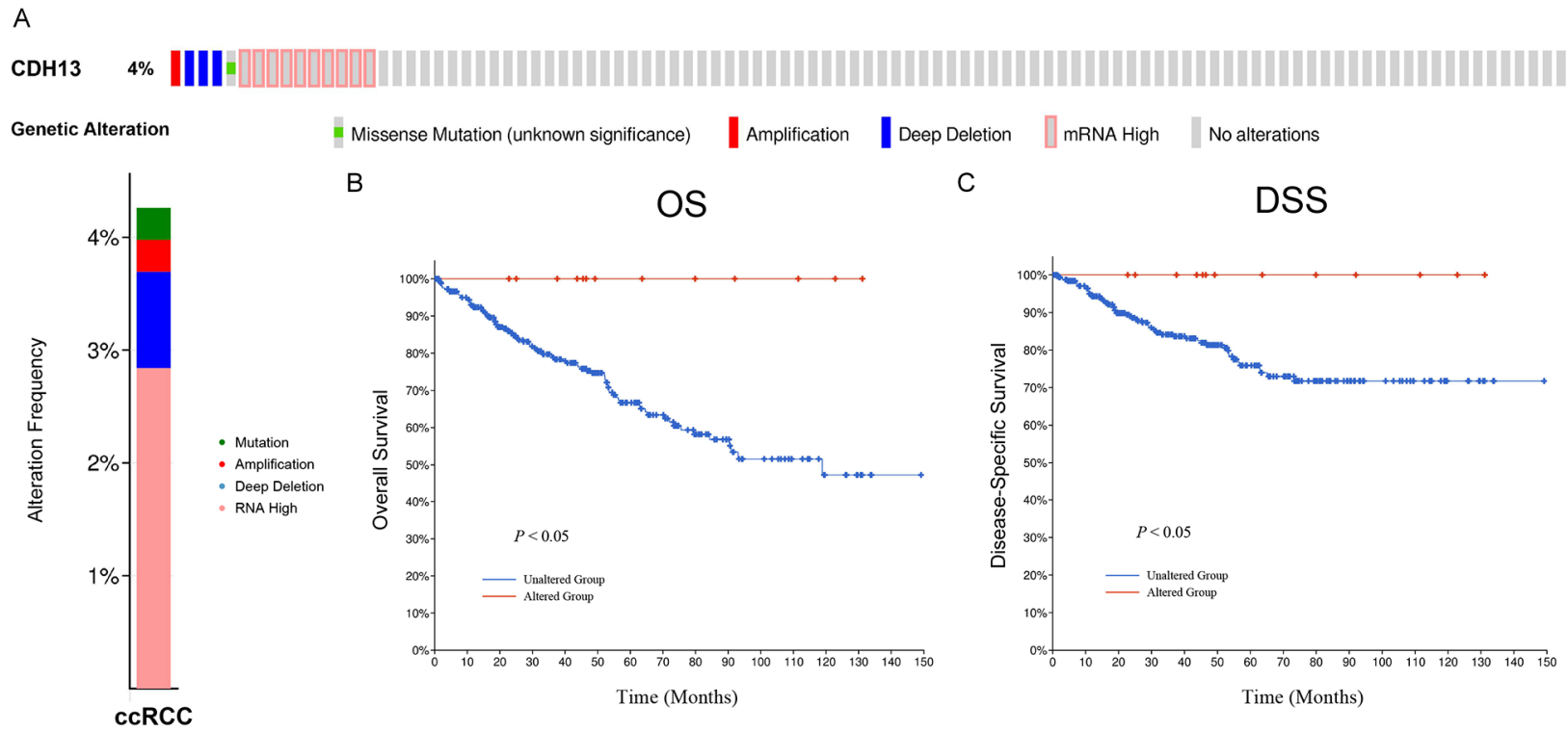

Figure 8. Genetic alterations of CDH13 in patients with ccRCC and association with OS and DSS of ccRCC patients (cBioPortal). A. Alteration frequency of CDH13 in ccRCC patients. B. Kaplan-Meier survival curve of genetic alteration of CDH13 and overall survival (OS). C. Kaplan-Meier survival curve of genetic alteration of CDH13 and disease specific survival (DSS).

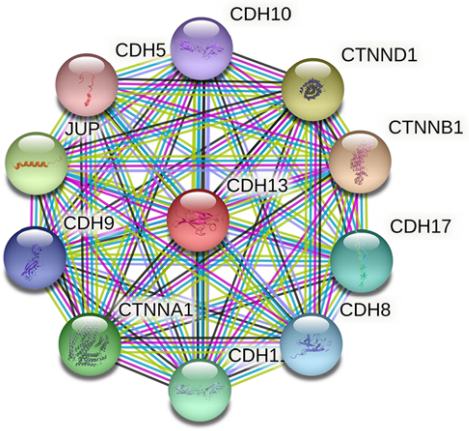

Gene symbol	Annotation	Score
CTNNB1	Catenin beta-1	0.939
CTNND1	Catenin delta-1	0.937
JUP	Junction plakoglobin	0.928
CTNNA1	Catenin alpha-1	0.927
CDH11	Cadherin-11	0.923
CDH17	Cadherin-17	0.922
CDH8	Cadherin-8	0.921
CDH9	Cadherin-9	0.920
CDH10	Cadherin-10	0.919
CDH5	Cadherin-5	0.916

Figure 9. Protein-protein interaction network of CDH13 and their co-expression scores (STRING).

of the Western blot analysis showed that the expression level of the CDH13 protein was upregulated in the ccRCC tissues. The results of immunohistochemical staining also showed that the expression level of CDH13 was significantly lower in the normal kidney tissues than that in the ccRCC tissues. Overall, the results based on the clinical samples confirmed the unique expression pattern of CDH13 recorded in the bioinformatic analysis.

The abnormal expression of CDH13 was also closely related to the clinicopathological factors of several cancer patients. Similarly, the upregulated level of CDH13 was strongly correlated with lower tumor grades and stages of ccRCC, which indicated that CDH13 might strongly influence tumor development and progression in ccRCC. The results of the immunohistochemical staining assay confirmed that the expression level of CDH13 was considerably higher in the low-grade ccRCC tissues than that in the high-grade ccRCC tissues. The results of the diagnostic analysis showed that CDH13 performed extremely well in the diagnosis of ccRCC. Thus, CDH13 might help clinicians in the pathological diagnosis of kidney tumors and metastatic tumors. It might complement preoperative imaging and the postoperative pathological diagnostic models used currently. Hence, CDH13 might provide personalized diagnostic solutions for ccRCC patients.

Several studies have reported that CDH13 is closely associated with angiogenesis and the ability of cancer cell lines to proliferate and migrate, which is crucial for cancer proliferation and metastasis [25, 49, 50]. Wang et al. conducted an in vitro study and found that the methylation of the promoter region of CDH13 restored the angiogenic, invasive, and migratory abilities of tumors [51]. Furthermore, the treatment of cancer cells with histone deacetylase inhibitors or demethylating agents could reactivate CDH13 expression and lead to tumor metastasis [51]. This might be related to the overexpression of CDH13 in endothelial cells, where CDH13 might stimulate the migration of endothelial cells and promote angiogenesis via vascular endothelial growth factor under pathological conditions [52]. In an in vivo study, CDH13 was found to promote tumor angiogenesis in a mouse model for cancer, where the deficiency of T-cadherin reduced tumor growth by limiting tumor angiogenesis [50]. Thus, the CDH13 gene strongly influences tumor development through multiple pathways and mechanisms. However, the prognostic value of CDH13 in ccRCC patients needs to be elucidated. We further investigated the prognostic value of CDH13 in ccRCC. The results of survival analyses indicated that an increase in the CDH13 level was correlated with better OS and PFS, partially because the ccRCC patients with higher levels of CDH13 had lower tumor grades and stages. Additionally, we constructed CDH13-based nomograms to develop an accurate method to predict the prognosis of ccRCC patients. We found that CDH13 might be an

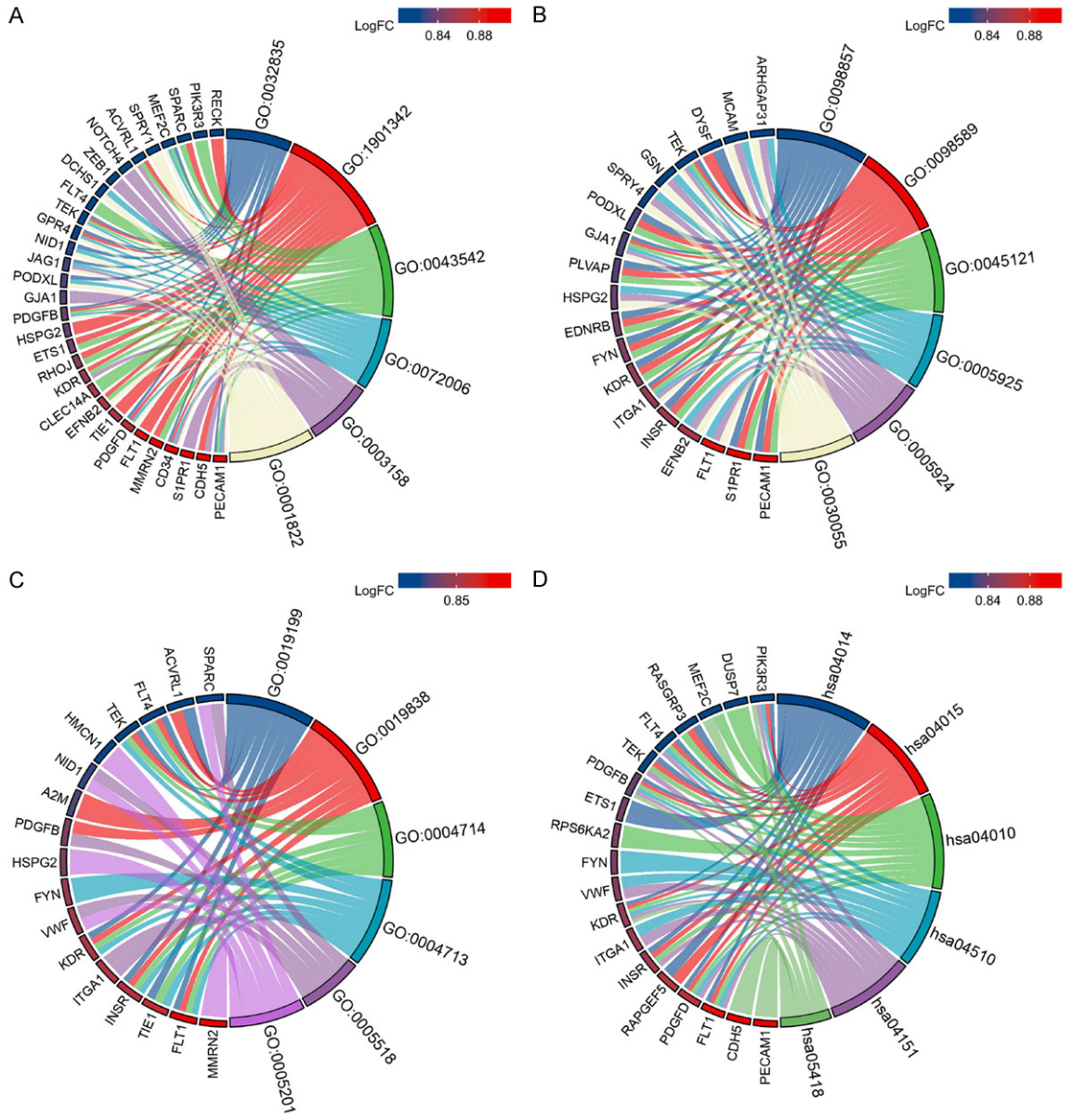

Figure 10. GO annotation and KEGG pathway enrichment analysis of CDH13 and its correlated genes in ccRCC. A. BP: Biological Process. B. CC: Cellular component. C. MF: Molecular funtion. D. Kyoto encyclopedia of genes and genomes (KEGG) pathways.

independent prognostic biomarker for ccRCC. Therefore, CDH13, along with other prognostic indicators, such as tumor stage, pathological grade, and lymph node metastasis, might help to predict the clinical outcome of ccRCC patients more accurately.

The tumor microenvironment (TME) has been studied extensively because it can promote tumor progression through multiple components, such as by enhancing proliferation, immune escape, and anti-apoptosis [53, 54]. Also, as potential targets for cancer therapy, tumor-infiltrating immune cells (TICs) are closely associated with the development of malignancies [55, 56]. Some patients with advanced ccRCC also benefit from immunotherapy [57, 58]. Therefore, we determined the correlation between CDH13 and immune cells, immune checkpoints, tumor lymphocyte infiltration, immunoinhibitors, immunostimulators, and major histocompatibility complex. The results showed that the expression of CDH13 was significantly correlated with the infiltration of CD8+ T

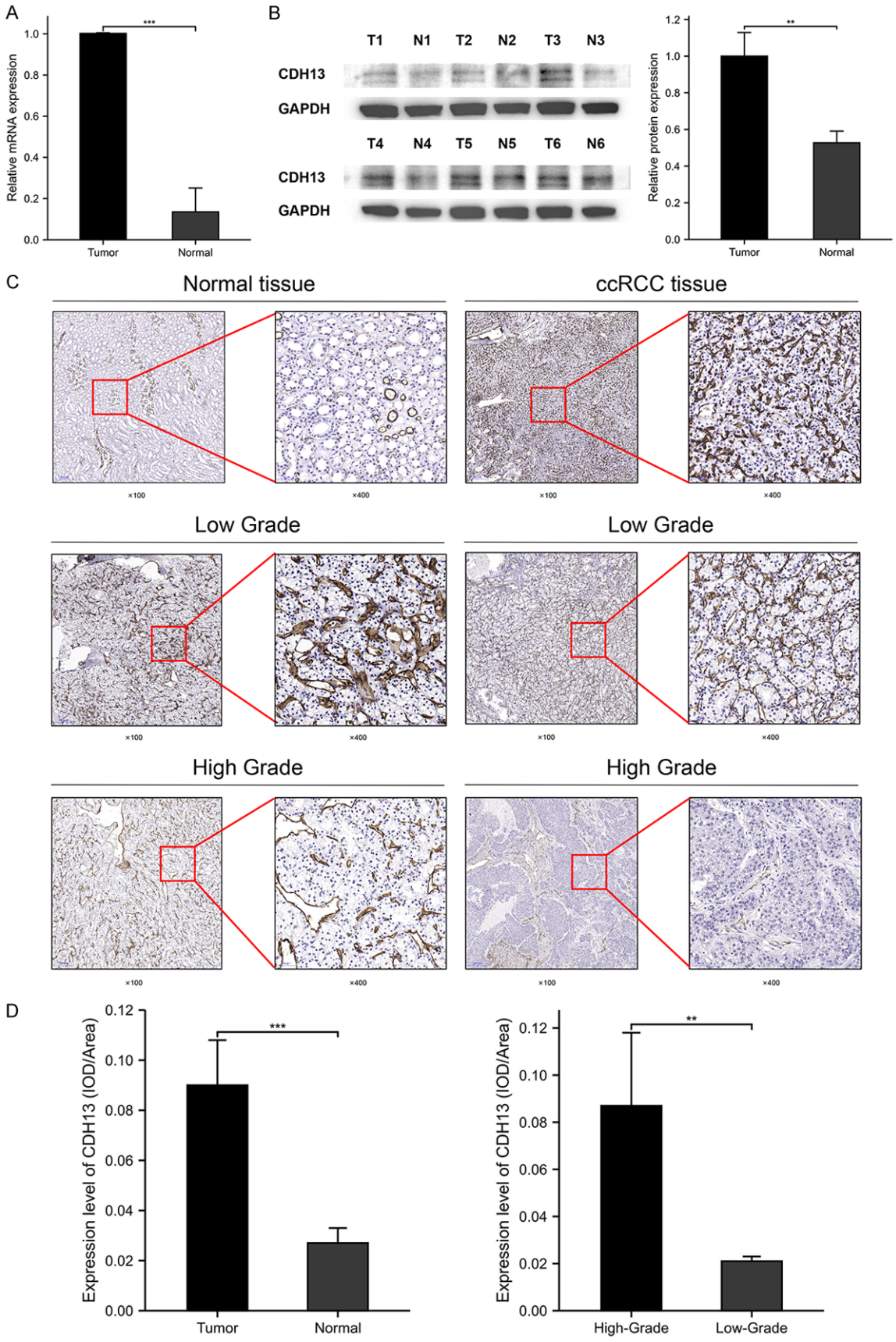
A
Relative mRNA expression
1.0
0.8
0.6
0.4
0.2
0.0
***
Tumor
Normal
B
T1 N1 T2 N2 T3 N3
CDH13
GAPDH
T4 N4 T5 N5 T6 N6
CDH13
GAPDH
Relative protein expression
1.2
1.0
0.8
0.6
0.4
0.2
0.0
**
Tumor
Normal
C
Normal tissue
ccRCC tissue
×100
×400
Low Grade
Low Grade
High Grade
High Grade
D
Expression level of CDH13 (IOD/Area)
0.12
0.10
0.08
0.06
0.04
0.02
0.00
***
Tumor
Normal
**
High-Grade
Low-Grade

Figure 11. CDH13 was upregulated in the ccRCC patients. A. Relative mRNA expression of CDH13 in the ccRCC tissues and adjacent normal kidney tissues. B. Western blot assay showed the protein expression level of CDH13 in the ccRCC tissues and adjacent normal kidney tissues. C. The typical immunohistochemistry images of CDH13 in the normal kidney tissues and ccRCC tissues. D. The expression level of CDH13 (IOD/Area) based on the immunohistochemistry images (***P < 0.001, **P < 0.01).

cells, CD4+ T cells, macrophages, neutrophils, dendritic cells, NK cells, mast cells, and pDCs. Additionally, the expression level of CDH13 showed a significant positive correlation with five immune checkpoints in ccRCC. The expression level of CDH13 was also significantly correlated with some immunosuppressive agents, immunostimulators, and major histocompatibility complexes. These results indicated that CDH13 might greatly contribute to the immune infiltration of ccRCC and influence the prognosis of ccRCC patients by converting anti-tumor cells into cancer cells and affecting the immune components of the TME.

The m6A modification is a novel regulatory mechanism for controlling gene expression in eukaryotic cells [59, 60]. The m6A modification is a reversible epigenetic modification, which is not only found in the mRNA but also in non-coding RNA; thus, it can modify RNA molecules [61, 62]. The m6A modification is present in almost all types of RNAs and dynamically regulates many physiological and pathological processes, including tumorigenesis [61, 63]. Therefore, in this study, we elucidated the relationship between m6A regulators and CDH13 and their prognostic value in ccRCC. The results indicated that the expression level of CDH13 was significantly correlated with the expression levels of METTL14, RBM15B, VIRMA, ZC3H13, FTO, YTHDF2, YTHDC1, and HNRNPC1. These m6A writers, erasers, and readers and the dynamic balance between the deposition and removal of m6A modifiers are important for maintaining appropriate m6A levels and gene expression in tissues and cells throughout the body. Their aberrant expression in ccRCC and close relationship with CDH13 might partially explain the unusual CDH13 expression pattern in ccRCC patients. Moreover, based on the 11 genes, including CDH13 and 10 m6A regulators, we constructed the prognostic model, which was significantly correlated with the prognosis of ccRCC patients. The methylation of the promoter region also strongly influenced the anomalous expression of CDH13 in patients with multiple cancers. The promoter of CDH13 is GC-rich and has CpG islands that are prone to methylation and the subsequent loss of gene functionality. A meta-analysis was conducted with 13 studies to determine the diagnostic ability of the methylation of CpG islands in the promoter regions of CDH13 in non-small cell lung cancer patients [64]. The pooled data showed that the methylation status of the CDH13 promoter was strongly associated with lung adenocarcinoma. The methylation status of CDH13 might be a diagnostic biomarker for the diagnosis of lung adenocarcinoma. Kontic et al. quantified the CpG methylation of CDH13 in the tumor tissues and normal lung tissues of 65 patients with non-small cell lung carcinoma by performing bisulfite pyrosequencing [65]. The results showed that the methylation of CDH13 was significantly higher in tumor tissues compared to that in normal lung tissues. Further analysis showed that the hypermethylation of CDH13 was correlated with the histology of the patients. Yuan et al. determined the methylation status of CDH13 in peripheral blood mononuclear cells by performing methylation-specific polymerase chain reactions [66]. The results showed that the methylation frequency of the CDH13 promoter was significantly higher in hepatocellular carcinoma patients than that in normal controls and patients with chronic hepatitis B. Additionally, the methylation of the CDH13 promoter was found to be an independent predictor of the prognosis of hepatocellular carcinoma and was associated with an increase in the risk among these patients. Based on the findings of the previous studies, we also analyzed the methylation of CpG islands in the promoter regions of CDH13 using the DNA methylation data of 319 ccRCC patients in the TCGA-KIRC dataset. The results indicated that cg03474070 was the core methylation region of CDH13, which was negatively associated with the expression level of the CDH13 mRNA and was also correlated with the OS of ccRCC patients. However, these results need to be confirmed by performing bisulfite pyrosequencing or methylation-specific polymerase chain reaction. Overall, the results of this study highlighted the epigenetic patterns

of CDH13 and the association of the prognosis of ccRCC patients with DNA methylation and m6A modification of CDH13.

Some studies have shown that the inactivation of the VHL gene is the predominant genetic alteration in ccRCC [67]. The inactivation of VHL was found in up to 91% of the patients with sporadic ccRCC due to methylation or mutation [68]. VHL targets hypoxia-inducible factors (HIF) for ubiquitin-mediated degradation through oxygen and iron-sensing mechanism, which in turn can disrupt important metabolic cascade reactions [69]. Under hypoxic conditions, prolyl hydroxylase cannot hydroxylate HIF-α. Mutated VHL cannot bind to HIF-α [70]. Thus, hypoxic conditions and mutations of VHL might reduce the degradation of HIF-α, thus, causing its accumulation. The accumulated HIF-α can regulate gene expression by binding to the hypoxia-responsive element in gene promoters. It affects several physiological processes, such as cell proliferation, angiogenesis, and apoptosis [69, 71]. However, previous studies did not investigate the genetic alteration rate of CDH13 in ccRCC patients. Thus, this study was the first to investigate the genetic alteration of CDH13 in ccRCC. The results showed that various CDH13 mutations were present in 4% of ccRCC patients. The results of the survival analysis suggested that the ccRCC patients without CDH13 mutations had worse OS and DSS. Overall, these results suggested that the clinical outcomes of ccRCC patients are influenced by the expression level and genetic mutations of CDH13.

To conduct the PPI analysis, we constructed a PPI network of CDH13 and predicted its functional partners. The results showed that most of the functional partners of the CDH13 gene were members of the cadherin family. The results of the functional enrichment analysis further confirmed that CDH13 is involved in glomerular development, transmembrane receptor protein kinase activity, focal adhesion, and multiple important signaling pathways in ccRCC. Thus, as an atypical member of the cadherin family, CDH13 strongly affects the maintenance of cell structure, regulation of cell growth, angiogenesis, cell recognition, cell adhesion, and intercellular signaling.

Our study had some limitations. First, we showed that CDH13 has a distinctive expression pattern in ccRCC; however, we did not determine the specific mechanism and the cause of this unusual expression pattern. Second, we did not investigate the exact mechanism of action of CDH13 in ccRCC, and further studies are needed to elucidate it. Finally, most findings of this study were based on bioinformatic analysis. Therefore, more studies with a larger clinical sample size are needed to support the results of this study.

In conclusion, in this study, we showed that CDH13 was upregulated in ccRCC tissues, and the expression level of CDH13 was closely associated with the clinicopathological characteristics, poor prognosis, and TME in ccRCC patients. Therefore, CDH13 might be a novel prognostic biomarker and therapeutic target for ccRCC patients. Our findings not only elucidated the molecular changes in ccRCC but also laid the foundation for further studies on the role of CDH13 in ccRCC.

Acknowledgements

This study was supported by the National Natural Science Foundation of China (No. 8197-0662), Scientific Research Funding Project of Returned Overseas Scholars of Shanxi Province (No. 2021-160), Shanxi “1331 project” Key Innovative Research Team (No. 3c332019001), and Sanming Project of Medicine in Shenzhen (No. SZSM202111003). The role of funders was in the design and writing the study. And we thank the editors and reviewers for providing very useful and professional comments during the revision of this study.

Disclosure of conflict of interest

None.

Address correspondence to: Dr. Bo Wu, Department of Urology, First Hospital of Shanxi Medical University, Taiyuan 030001, Shanxi, China. E-mail: 13803466385@163.com

References

[1] Siegel RL, Miller KD, Fuchs HE and Jemal A. Cancer statistics, 2022. CA Cancer J Clin 2022; 72: 7-33.

[2] Capitanio U, Bensalah K, Bex A, Boorjian SA, Bray F, Coleman J, Gore JL, Sun M, Wood C and Russo P. Epidemiology of renal cell carcinoma. Eur Urol 2019; 75: 74-84.

[3] Ferlay J, Colombet M, Soerjomataram I, Dyba T, Randi G, Bettio M, Gavin A, Visser O and Bray F. Cancer incidence and mortality patterns in Europe: estimates for 40 countries and 25 major cancers in 2018. Eur J Cancer 2018; 103: 356-387.

[4] Moch H, Cubilla A, Humphrey P, Reuter V and Ulbright T. The 2016 WHO classification of tumours of the urinary system and male genital organs-part a: renal, penile, and testicular tumours. Eur Urol 2016; 70: 93-105.

[5] Srigley JR, Delahunt B, Eble JN, Egevad L, Epstein JI, Grignon D, Hes O, Moch H, Montironi R, Tickoo SK, Zhou M and Argani P. The international society of urological pathology (ISUP) vancouver classification of renal neoplasia. Am J Surg Pathol 2013; 37: 1469-1489.

[6] Jayson M and Sanders H. Increased incidence of serendipitously discovered renal cell carcinoma. Urology 1998; 51: 203-205.

[7] Vasudev NS, Wilson M, Stewart GD, Adeyoju A, Cartledge J, Kimuli M, Datta S, Hanbury D, Hrouda D, Oades G, Patel P, Soomro N, Sullivan M, Webster J, Selby PJ and Banks RE. Challenges of early renal cancer detection: symptom patterns and incidental diagnosis rate in a multicentre prospective UK cohort of patients presenting with suspected renal cancer. BMJ Open 2020; 10: e035938.

[8] Patard JJ, Leray E, Rodriguez A, Rioux-Leclercq N, Guillé F and Lobel B. Correlation between symptom graduation, tumor characteristics and survival in renal cell carcinoma. Eur Urol 2003; 44: 226-232.

[9] Campbell S, Uzzo R, Allaf M, Bass E, Cadeddu J, Chang A, Clark P, Davis B, Derweesh I, Giambarresi L, Gervais D, Hu S, Lane B, Leibovich B and Pierorazio P. Renal mass and localized renal cancer: AUA guideline. J Urol 2017; 198: 520-529.

[10] Ljungberg B, Albiges L, Abu-Ghanem Y, Bensalah K, Dabestani S, Fernández-Pello S, Giles R, Hofmann F, Hora M, Kuczyk M, Kuusk T, Lam T, Marconi L, Merseburger A, Powles T, Staehler M, Tahbaz R, Volpe A and Bex A. European association of urology guidelines on renal cell carcinoma: the 2019 update. Eur Urol 2019; 75: 799-810.

[11] Ray S, Cheaib JG, Biles MJ, Pineault KG, Johnson MH, Ged YMA, Markowski MC, Singla N, Allaf ME and Pierorazio PM. Local and regional recurrences of clinically localized renal cell carcinoma after nephrectomy: a 15 year institutional experience with prognostic features and oncologic outcomes. Urology 2021; 154: 201-207.

[12] Gorin MA, Patel HD, Rowe SP, Hahn NM, Hammers HJ, Pons A, Trock BJ, Pierorazio PM, Nirschl TR, Salles DC, Stein JE, Lotan TL, Taube JM, Drake CG and Allaf ME. Neoadjuvant nivolumab in patients with high-risk nonmetastatic renal cell carcinoma. Eur Urol Oncol 2022; 5: 113-117.

[13] Johnson DC, Vukina J, Smith AB, Meyer AM, Wheeler SB, Kuo TM, Tan HJ, Woods ME, Raynor MC, Wallen EM, Pruthi RS and Nielsen ME. Preoperatively misclassified, surgically removed benign renal masses: a systematic review of surgical series and United States population level burden estimate. J Urol 2015; 193: 30-35.

[14] Roussel E, Capitanio U, Kutikov A, Oosterwijk E, Pedrosa I, Rowe SP and Gorin MA. Novel imaging methods for renal mass characterization: a collaborative review. Eur Urol 2022; 81: 476-488.

[15] Ward RD, Tanaka H, Campbell SC and Remer EM. 2017 AUA renal mass and localized renal cancer guidelines: imaging implications. Radiographics 2018; 38: 2021-2033.

[16] Campbell SC, Clark PE, Chang SS, Karam JA, Souter L and Uzzo RG. Renal mass and localized renal cancer: evaluation, management, and follow-up: AUA guideline: part I. J Urol 2021; 206: 199-208.

[17] Cotta BH, Meagher MF, Bradshaw A, Ryan ST, Rivera-Sanfeliz G and Derweesh IH. Percutaneous renal mass biopsy: historical perspective, current status, and future considerations. Expert Rev Anticancer Ther 2019; 19: 301-308.

[18] Lee S. H-cadherin, a novel cadherin with growth inhibitory functions and diminished expression in human breast cancer. Nat Med 1996; 2: 776-782.

[19] Angst BD, Marcozzi C and Magee AI. The cadherin superfamily: diversity in form and function. J Cell Sci 2001; 114: 629-641.

[20] Philippova M, Joshi MB, Kyriakakis E, Pfaff D, Erne P and Resink TJ. A guide and guard: the many faces of T-cadherin. Cell Signal 2009; 21: 1035-1044.

[21] Hulpiau P and van Roy F. Molecular evolution of the cadherin superfamily. Int J Biochem Cell Biol 2009; 41: 349-369.

[22] Andreeva AV and Kutuzov MA. Cadherin 13 in cancer. Genes Chromosomes Cancer 2010; 49: 775-790.

[23] Philippova M, Ivanov D, Joshi MB, Kyriakakis E, Rupp K, Afonyushkin T, Bochkov V, Erne P and Resink TJ. Identification of proteins associating with glycosylphosphatidylinositol-anchored T-cadherin on the surface of vascular endothelial cells: role for Grp78/BiP in T-cadherin-dependent cell survival. Mol Cell Biol 2008; 28: 4004-4017.

[24] Karnati HK, Panigrahi MK, Li Y, Tweedie D and Greig NH. Adiponectin as a potential therapeutic target for prostate cancer. Curr Pharm Des 2017; 23: 4170-4179.

[25] Zheng W, Zhang S, Guo H, Chen X, Huang Z, Jiang S and Li M. Multi-omics analysis of tumor angiogenesis characteristics and potential epigenetic regulation mechanisms in renal clear cell carcinoma. Cell Commun Signal 2021; 19: 39.
[26] Lin Y, Sun G, Liu X, Chen Y and Zhang C. Clinical significance of T-cadherin tissue expression in patients with bladder transitional cell carcinoma. Urol Int 2011; 86: 340-345.
[27] Wang Q, Zhang X, Song X and Zhang L. Overexpression of T-cadherin inhibits the proliferation of oral squamous cell carcinoma through the PI3K/AKT/mTOR intracellular signalling pathway. Arch Oral Biol 2018; 96: 74-79.
[28] Xu D, Yuan H, Meng Z, Yang C, Li Z, Li M, Zhang Z, Gan Y and Tu H. Cadherin 13 inhibits pancreatic cancer progression and epithelial-mesenchymal transition by Wnt/β-catenin signaling. J Cancer 2020; 11: 2101-2112.
[29] Rhodes DR, Yu J, Shanker K, Deshpande N, Varambally R, Ghosh D, Barrette T, Pandey A and Chinnaiyan AM. ONCOMINE: a cancer microarray database and integrated data-mining platform. Neoplasia 2004; 6: 1-6.
[30] Tang Z, Li C, Kang B, Gao G, Li C and Zhang Z. GEPIA: a web server for cancer and normal gene expression profiling and interactive analyses. Nucleic Acids Res 2017; 45: W98-W102.
[31] Wang Z, Jensen MA and Zenklusen JC. A practical guide to The Cancer Genome Atlas (TCGA). Methods Mol Biol 2016; 1418: 111-141.
[32] von Roemeling CA, Radisky DC, Marlow LA, Cooper SJ, Grebe SK, Anastasiadis PZ, Tun HW and Copland JA. Neuronal pentraxin 2 supports clear cell renal cell carcinoma by activating the AMPA-selective glutamate receptor-4. Cancer Res 2014; 74: 4796-4810.
[33] Wozniak MB, Le Calvez-Kelm F, Abedi-Ardekani B, Byrnes G, Durand G, Carreira C, Michelon J, Janout V, Holcatova I, Foretova L, Brisuda A, Lesueur F, McKay J, Brennan P and Scelo G. Integrative genome-wide gene expression profiling of clear cell renal cell carcinoma in Czech Republic and in the United States. PLoS One 2013; 8: e57886.
[34] Chen F, Chandrashekar DS, Varambally S and Creighton CJ. Pan-cancer molecular subtypes revealed by mass-spectrometry-based proteomic characterization of more than 500 human cancers. Nat Commun 2019; 10: 5679.
[35] Thul PJ, Åkesson L, Wiking M, Mahdessian D, Geladaki A, Ait Blal H, Alm T, Asplund A, Björk L, Breckels LM, Bäckström A, Danielsson F, Fagerberg L, Fall J, Gatto L, Gnann C, Hober S, Hjelmare M, Johansson F, Lee S, Lindskog C, Mulder J, Mulvey CM, Nilsson P, Oksvold P, Rockberg J, Schutten R, Schwenk JM, Sivertsson Å, Sjöstedt E, Skogs M, Stadler C, Sullivan DP, Tegel H, Winsnes C, Zhang C, Zwahlen M, Mardinoglu A, Pontén F, von Feilitzen K, Lilley KS, Uhlén M and Lundberg E. A subcellular map of the human proteome. Science 2017; 356: 3321.
[36] Jumper J, Evans R, Pritzel A, Green T, Figurnov M, Ronneberger O, Tunyasuvunakool K, Bates R, Žídek A, Potapenko A, Bridgland A, Meyer C, Kohl SAA, Ballard AJ, Cowie A, Romera-Paredes B, Nikolov S, Jain R, Adler J, Back T, Petersen S, Reiman D, Clancy E, Zielinski M, Steinegger M, Pacholska M, Berghammer T, Bodenstein S, Silver D, Vinyals O, Senior AW, Kavukcuoglu K, Kohli P and Hassabis D. Highly accurate protein structure prediction with AlphaFold. Nature 2021; 596: 583-589.
[37] Chandrashekar DS, Bashel B, Balasubramanya SAH, Creighton CJ, Ponce-Rodriguez I, Chakravarthi B and Varambally S. UALCAN: a portal for facilitating tumor subgroup gene expression and survival analyses. Neoplasia 2017; 19: 649-658.
[38] Li T, Fan J, Wang B, Traugh N, Chen Q, Liu JS, Li B and Liu XS. TIMER: a web server for comprehensive analysis of tumor-infiltrating immune cells. Cancer Res 2017; 77: e108-e110.
[39] Hänzelmann S, Castelo R and Guinney J. GSVA: gene set variation analysis for microarray and RNA-seq data. BMC Bioinformatics 2013; 14: 7.
[40] Bindea G, Mlecnik B, Tosolini M, Kirilovsky A, Waldner M, Obenauf AC, Angell H, Fredriksen T, Lafontaine L, Berger A, Bruneval P, Fridman WH, Becker C, Pagès F, Speicher MR, Trajanoski Z and Galon J. Spatiotemporal dynamics of intratumoral immune cells reveal the immune landscape in human cancer. Immunity 2013; 39: 782-795.
[41] Ru B, Wong CN, Tong Y, Zhong JY, Zhong SSW, Wu WC, Chu KC, Wong CY, Lau CY, Chen I, Chan NW and Zhang J. TISIDB: an integrated repository portal for tumor-immune system interactions. Bioinformatics 2019; 35: 4200-4202.
[42] Goldman MJ, Craft B, Hastie M, Repečka K, McDade F, Kamath A, Banerjee A, Luo Y, Rogers D, Brooks AN, Zhu J and Haussler D. Visualizing and interpreting cancer genomics data via the Xena platform. Nat Biotechnol 2020; 38: 675-678.
[43] Gao J, Aksoy BA, Dogrusoz U, Dresdner G, Gross B, Sumer SO, Sun Y, Jacobsen A, Sinha R, Larsson E, Cerami E, Sander C and Schultz N. Integrative analysis of complex cancer genomics and clinical profiles using the cBioPortal. Sci Signal 2013; 6: pl1.
[44] Szklarczyk D, Gable AL, Nastou KC, Lyon D, Kirsch R, Pyysalo S, Doncheva NT, Legeay M, Fang T, Bork P, Jensen LJ and von Mering C. The STRING database in 2021: customizable

protein-protein networks, and functional characterization of user-uploaded gene/measurement sets. Nucleic Acids Res 2021; 49: D605-612.
[45] Zhou Y, Zhou B, Pache L, Chang M, Khodabakhshi AH, Tanaseichuk O, Benner C and Chanda SK. Metascape provides a biologist-oriented resource for the analysis of systems-level datasets. Nat Commun 2019; 10: 1523.
[46] Di Palo A, Siniscalchi C, Polito R, Nigro E, Russo A, Daniele A and Potenza N. MicroRNA-377-3p downregulates the oncosuppressor T-cadherin in colorectal adenocarcinoma cells. Cell Biol Int 2021; 45: 1797-1803.
[47] Dasen B, Vlajnic T, Mengus C, Ruiz C, Bubendorf L, Spagnoli G, Wyler S, Erne P, Resink TJ and Philippova M. T-cadherin in prostate cancer: relationship with cancer progression, differentiation and drug resistance. J Pathol Clin Res 2017; 3: 44-57.
[48] Wang Y, Zhang L, Yang J, Li B and Wang J. CDH13 promoter methylation regulates cisplatin resistance of non-small cell lung cancer cells. Oncol Lett 2018; 16: 5715-5722.
[49] Kyriakakis E, Maslova K, Philippova M, Pfaff D, Joshi MB, Buechner SA, Erne P and Resink TJ. T-cadherin is an auxiliary negative regulator of EGFR pathway activity in cutaneous squamous cell carcinoma: impact on cell motility. J Invest Dermatol 2012; 132: 2275-2285.
[50] Hebbard LW, Garlatti M, Young LJ, Cardiff RD, Oshima RG and Ranscht B. T-cadherin supports angiogenesis and adiponectin association with the vasculature in a mouse mammary tumor model. Cancer Res 2008; 68: 1407-1416.
[51] Wang M, Long K, Li E, Li L, Li B, Ci S, He L, Pan F, Hu Z and Guo Z. DNA polymerase beta modulates cancer progression via enhancing CDH13 expression by promoter demethylation. Oncogene 2020; 39: 5507-5519.
[52] Philippova M, Banfi A, Ivanov D, Gianni-Barrera R, Allenspach R, Erne P and Resink T. Atypical GPI-anchored T-cadherin stimulates angiogenesis in vitro and in vivo. Arterioscler Thromb Vasc Biol 2006; 26: 2222-2230.
[53] Wu T and Dai Y. Tumor microenvironment and therapeutic response. Cancer Lett 2017; 387: 61-68.
[54] Hinshaw DC and Shevde LA. The tumor microenvironment innately modulates cancer progression. Cancer Res 2019; 79: 4557-4566.
[55] Gajewski TF, Schreiber H and Fu YX. Innate and adaptive immune cells in the tumor microenvironment. Nat Immunol 2013; 14: 1014-1022.
[56] Kumar S, Singh SK, Rana B and Rana A. Tumor-infiltrating CD8(+) T cell antitumor efficacy and exhaustion: molecular insights. Drug Discov Today 2021; 26: 951-967.
[57] Motzer RJ, Jonasch E, Boyle S, Carlo MI, Manley B, Agarwal N, Alva A, Beckermann K, Choueiri TK, Costello BA, Derweesh IH, Desai A, George S, Gore JL, Haas N, Hancock SL, Kyriakopoulos C, Lam ET, Lau C, Lewis B, Madoff DC, McCreery B, Michaelson MD, Mortazavi A, Nandagopal L, Pierorazio PM, Plimack ER, Ponsky L, Ramalingam S, Shuch B, Smith ZL, Somer B, Sosman J, Dwyer MA and Motter AD. NCCN guidelines insights: kidney cancer, version 1.2021. J Natl Compr Canc Netw 2020; 18: 1160-1170.
[58] Bedke J, Albiges L, Capitanio U, Giles RH, Hora M, Lam TB, Ljungberg B, Marconi L, Klatte T, Volpe A, Abu-Ghanem Y, Dabestani S, Fernández-Pello S, Hofmann F, Kuusk T, Tahbaz R, Powles T and Bex A. Updated european association of urology guidelines on renal cell carcinoma: nivolumab plus cabozantinib joins immune checkpoint inhibition combination therapies for treatment-naïve metastatic clear-cell renal cell carcinoma. Eur Urol 2021; 79: 339-342.
[59] Liu ZX, Li LM, Sun HL and Liu SM. Link between m6A modification and cancers. Front Bioeng Biotechnol 2018; 6: 89.
[60] Gao R, Ye M, Liu B, Wei M, Ma D and Dong K. M6A modification: a double-edged sword in tumor development. Front Oncol 2021; 11: 679367.
[61] Huang H, Weng H and Chen J. M6A modification in coding and non-coding RNAs: roles and therapeutic implications in cancer. Cancer Cell 2020; 37: 270-288.
[62] Qin S, Mao Y, Wang H, Duan Y and Zhao L. The interplay between m6A modification and non-coding RNA in cancer stemness modulation: mechanisms, signaling pathways, and clinical implications. Int J Biol Sci 2021; 17: 2718-2736.
[63] Chen C, Guo Y, Guo Y, Wu X, Si C, Xu Y, Kang Q and Sun Z. M6A modification in non-coding RNA: the role in cancer drug resistance. Front Oncol 2021; 11: 746789.
[64] Pu W, Geng X, Chen S, Tan L, Tan Y, Wang A, Lu Z, Guo S, Chen X and Wang J. Aberrant methylation of CDH13 can be a diagnostic biomarker for lung adenocarcinoma. J Cancer 2016; 7: 2280-2289.
[65] Kontic M, Stojsic J, Jovanovic D, Bunjevacki V, Ognjanovic S, Kuriger J, Puumala S and Nelson HH. Aberrant promoter methylation of CDH13 and MGMT genes is associated with clinicopathologic characteristics of primary non-small-cell lung carcinoma. Clin Lung Cancer 2012; 13: 297-303.
[66] Yuan XD, Wang JW, Fang Y, Qian Y, Gao S, Fan YC and Wang K. Methylation status of the T-cadherin gene promotor in peripheral blood

mononuclear cells is associated with HBV-related hepatocellular carcinoma progression. Pathol Res Pract 2020; 216: 152914.
[67] Linehan WM and Ricketts CJ. The cancer genome atlas of renal cell carcinoma: findings and clinical implications. Nat Rev Urol 2019; 16: 539-552.
[68] Nickerson ML, Jaeger E, Shi Y, Durocher JA, Mahurkar S, Zaridze D, Matveev V, Janout V, Kollarova H, Bencko V, Navratilova M, Szeszenia-Dabrowska N, Mates D, Mukeria A, Holcatova I, Schmidt LS, Toro JR, Karami S, Hung R, Gerard GF, Linehan WM, Merino M, Zbar B, Boffetta P, Brennan P, Rothman N, Chow WH, Waldman FM and Moore LE. Improved identification of von Hippel-Lindau gene alterations in clear cell renal tumors. Clin Cancer Res 2008; 14: 4726-4734.
[69] Linehan WM, Srinivasan R and Schmidt LS. The genetic basis of kidney cancer: a metabolic disease. Nat Rev Urol 2010; 7: 277-285.
[70] Guo K, Wei Y, Wang Z, Zhang X, Zhang X, Liu X, Wu W, Wu Z, Zhang L and Cui CP. Deubiquitylase OTUD6B stabilizes the mutated pVHL and suppresses cell migration in clear cell renal cell carcinoma. Cell Death Dis 2022; 13: 97.
[71] Linehan WM, Bratslavsky G, Pinto PA, Schmidt LS, Neckers L, Bottaro DP and Srinivasan R. Molecular diagnosis and therapy of kidney cancer. Annu Rev Med 2010; 61: 329-343.

Table S1. The primers designed for this study

Gene	Sequence	Product
CDH13	F: 5'-TGTCCCAAGACAAAAGAGGTCC-3'	100 bp
	R: 5'-ACTATCGACTACCTTGCCAACAT-3'	
GAPDH	F: 5'-GTCCACCACCCTGTTGCTGTA-3'	111 bp
	R: 5'-ACCCACTCCTCCACCTTTGA-3'	

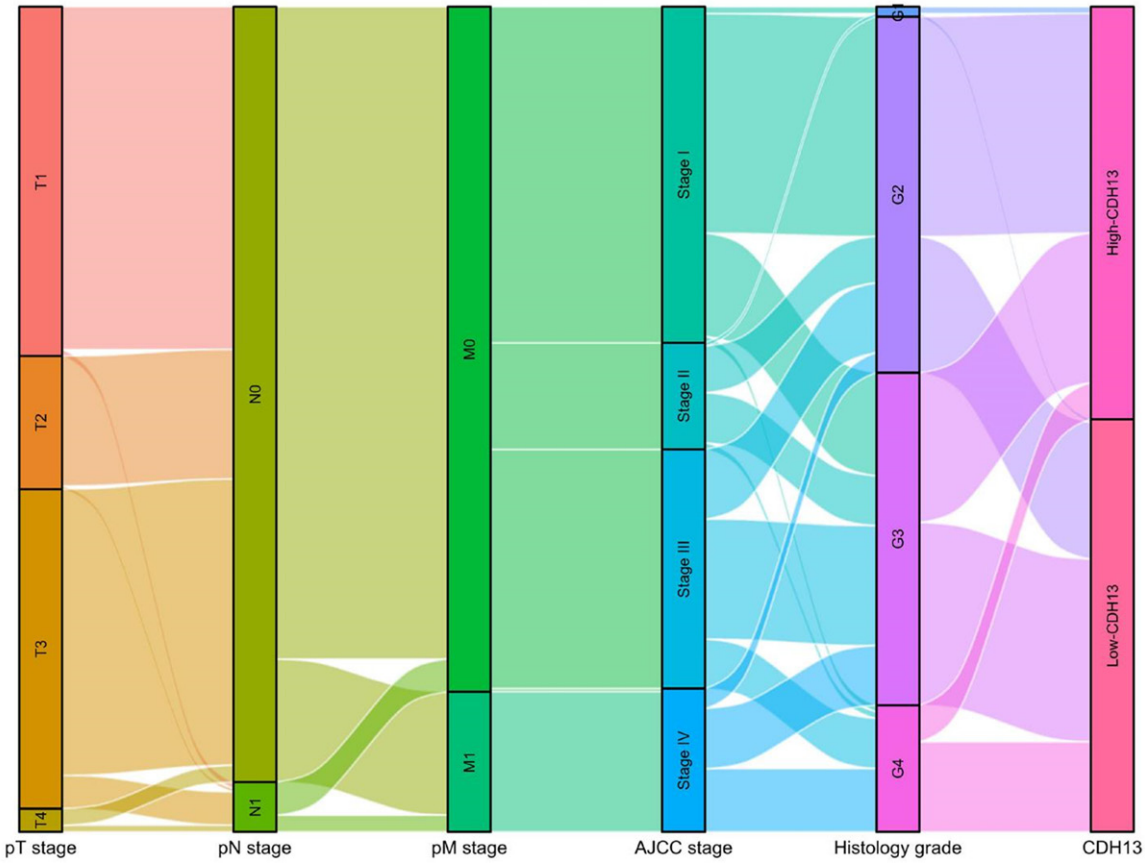

Figure S1. The sankey plot of the clinicopathological characteristics of ccRCC patients from TCGA-KIRC datasets.

A

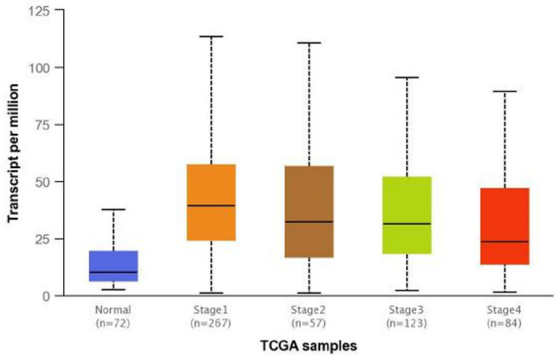
Expression of CDH13 in KIRC based on individual cancer stages
Transcript per million
125
100
75
50
25
0
Normal (n=72)
Stage1 (n=267)
Stage2 (n=57)
Stage3 (n=123)
Stage4 (n=84)
TCGA samples

B

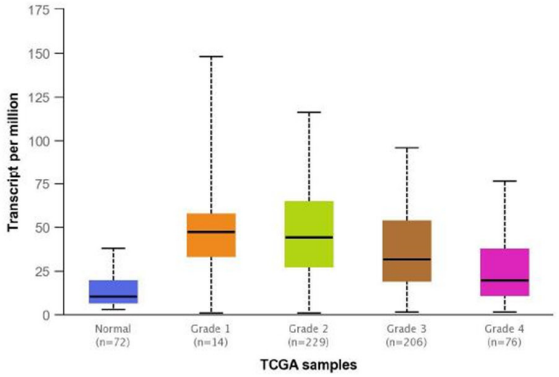
Expression of CDH13 in KIRC based on tumor grade
Transcript per million
175
150
125
100
75
50
25
0
Normal (n=72)
Grade 1 (n=14)
Grade 2 (n=229)
Grade 3 (n=206)
Grade 4 (n=76)
TCGA samples

C

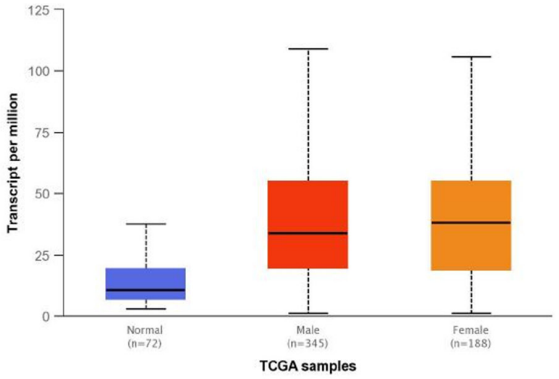
Expression of CDH13 in KIRC based on patient's gender
Transcript per million
125
100
75
50
25
0
Normal (n=72)
Male (n=345)
Female (n=188)
TCGA samples

D

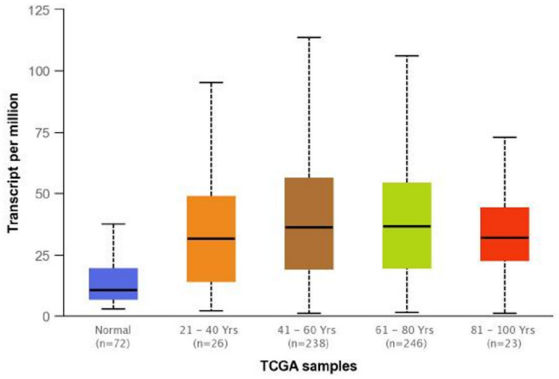
Expression of CDH13 in KIRC based on patient's age
Transcript per million
125
100
75
50
25
0
Normal (n=72)
21 – 40 Yrs (n=26)
41 – 60 Yrs (n=238)
61 – 80 Yrs (n=246)
81 – 100 Yrs (n=23)
TCGA samples

E

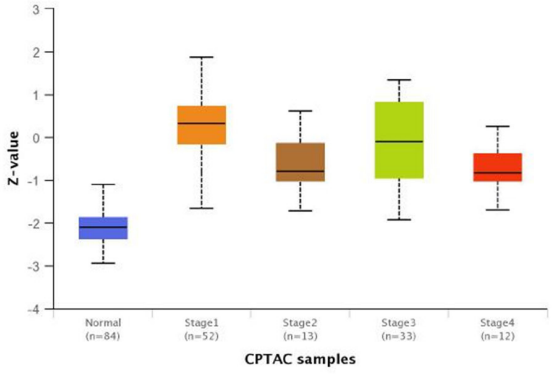
Protein expression of CDH13 in Clear cell RCC
Z-value
3
2
1
0
-1
-2
-3
-4
Normal (n=84)
Stage1 (n=52)
Stage2 (n=13)
Stage3 (n=33)
Stage4 (n=12)
CPTAC samples

F

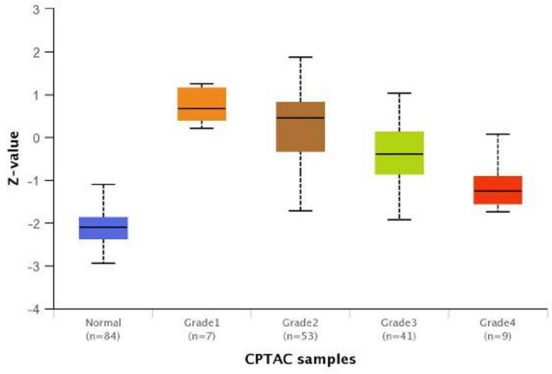
Protein expression of CDH13 in Clear cell RCC
Z-value
3
2
1
0
-1
-2
-3
-4
Normal (n=84)
Grade1 (n=7)
Grade2 (n=53)
Grade3 (n=41)
Grade4 (n=9)
CPTAC samples

G

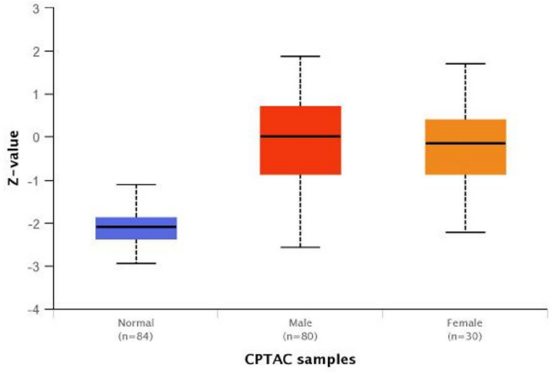
Protein expression of CDH13 in Clear cell RCC
Z-value
3
2
1
0
-1
-2
-3
-4
Normal (n=84)
Male (n=80)
Female (n=30)
CPTAC samples

H

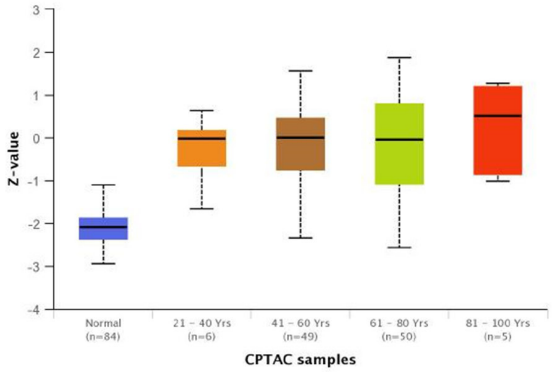
Protein expression of CDH13 in Clear cell RCC
Z-value
3
2
1
0
-1
-2
-3
-4
Normal (n=84)
21 – 40 Yrs (n=6)
41 – 60 Yrs (n=49)
61 – 80 Yrs (n=50)
81 – 100 Yrs (n=5)
CPTAC samples

Figure S2. Association of mRNA and protein expression level of CDH13 and clinicopathological features in ccRCC patients (UALCAN and CPTAC). A. Association of CDH13 mRNA expression and ccRCC stages. B. CDH13 and tumor grades. C. CDH13 and gender of patiens. D. CDH13 and age of patients. E. Association of CDH13 protein expression and ccRCC stages. F. CDH13 and tumor grades. G. CDH13 and gender of patiens. H. CDH13 and age of patients.

Table S2. Association of the expression level of CDH13 and clinicopathological features in ccRCC patients (UALCAN and CPTAC)

Expression level	Comparison	Statistical significance
mRNA level	Normal-vs-Stage 1	< 1E-12
	Normal-vs-Stage 2	6.149E-08
	Normal-vs-Stage 3	< 1E-12
	Normal-vs-Stage 4	2.218E-09
	Stage 1-vs-Stage 2	2.604E-01
	Stage 1-vs-Stage 3	9.283E-03
	Stage 1-vs-Stage 4	1.594E-05
	Stage 2-vs-Stage 3	6.088E-01
	Stage 2-vs-Stage 4	7.262E-02
	Stage 3-vs-Stage 4	5.536E-02
	Normal-vs-Grade 1	3.060E-03
	Normal-vs-Grade 2	1.624E-12
	Normal-vs-Grade 3	1.624E-12
	Normal-vs-Grade 4	1.469E-06
	Grade 1-vs-Grade 2	1.617E-01
	Grade 1-vs-Grade 3	4.542E-02
	Grade 1-vs-Grade 4	1.694E-02
	Grade 2-vs-Grade 3	1.524E-05
	Grade 2-vs-Grade 4	1.970E-09
	Grade 3-vs-Grade 4	4.356E-03
	Normal-vs-Male	1.624E-12
	Normal-vs-Female	< 1E-12
	Male-vs-Female	7.873E-01
	Normal-vs-Age (21-40 Yrs)	2.442E-04
	Normal-vs-Age (41-60 Yrs)	< 1E-12
	Normal-vs-Age (61-80 Yrs)	< 1E-12
	Normal-vs-Age (81-100 Yrs)	1.027E-04
	Age (21-40 Yrs)-vs-Age (41-60 Yrs)	9.419E-01
	Age (21-40 Yrs)-vs-Age (61-80 Yrs)	6.279E-01
	Age (21-40 Yrs)-vs-Age (81-100 Yrs)	2.430E-01
	Age (41-60 Yrs)-vs-Age (61-80 Yrs)	2.365E-01
	Age (41-60 Yrs)-vs-Age (81-100 Yrs)	4.116E-02
	Age (61-80 Yrs)-vs-Age (81-100 Yrs)	2.526E-01
Protein level	Normal-vs-Stage 1	2.263E-21
	Normal-vs-Stage 2	3.918E-06
	Normal-vs-Stage 3	5.139E-12
	Normal-vs-Stage 4	4.322E-05
	Stage 1-vs-Stage 2	9.645E-03
	Stage 1-vs-Stage 3	2.965E-01
	Stage 1-vs-Stage 4	3.185E-02
	Stage 2-vs-Stage 3	1.198E-01

Stage 2-vs-Stage 4	9.119E-01
Stage 3-vs-Stage 4	2.018E-01
Normal-vs-Grade 1	1.779E-03
Normal-vs-Grade 2	5.131E-22
Normal-vs-Grade 3	1.005E-17
Normal-vs-Grade 4	7.418E-03
Grade 1-vs-Grade 2	6.659E-01
Grade 1-vs-Grade 3	1.571E-01
Grade 1-vs-Grade 4	5.182E-02
Grade 2-vs-Grade 3	5.784E-03
Grade 2-vs-Grade 4	1.755E-02
Grade 3-vs-Grade 4	2.104E-01
Normal-vs-Male	4.570E-29
Normal-vs-Female	6.366E-12
Male-vs-Female	4.879E-01
Normal-vs-Age (21-40 Yrs)	3.133E-03
Normal-vs-Age (41-60 Yrs)	1.969E-22
Normal-vs-Age (61-80 Yrs)	9.519E-16
Normal-vs-Age (81-100 Yrs)	9.753E-03
Age (21-40 Yrs)-vs-Age (41-60 Yrs)	7.137E-01
Age (21-40 Yrs)-vs-Age (61-80 Yrs)	7.926E-01
Age (21-40 Yrs)-vs-Age (81-100 Yrs)	4.282E-01
Age (41-60 Yrs)-vs-Age (61-80 Yrs)	8.615E-01
Age (41-60 Yrs)-vs-Age (81-100 Yrs)	5.092E-01
Age (61-80 Yrs)-vs-Age (81-100 Yrs)	4.775E-01

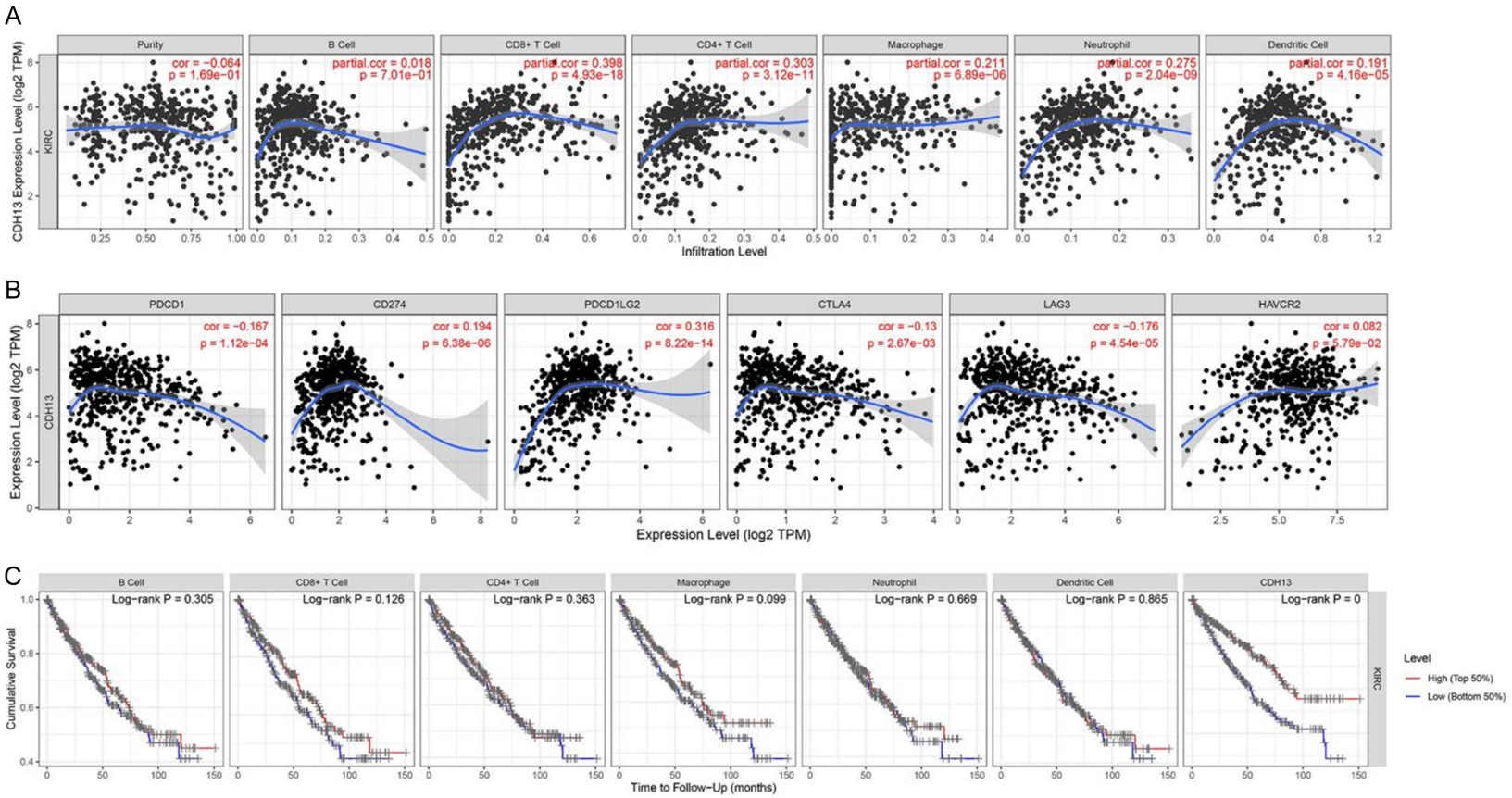

Figure S3. A. Correlation between CDH13 expression and six tumor-infiltrating immune cells in ccRCC. B. Correlation between CDH13 expression and six immune checkpoints in ccRCC. C. Kaplan-Meier survival curve of CDH13 expression and six tumor-infiltrating immune cells (TIMER).

Table S3. The cox proportianal hazard model of six tumor-infiltrating immune cells and CDH13 in ccRCC patients (TIMER)

Factors	*HR*	95% *CI*	*p* value
B- cell	0.290	0.015-5.638	0.414
CD8- T cell	0.365	0.081-1.650	0.190
CD4- T cell	1.392	0.109-17.780	0.799
Macrophage	0.080	0.009-0.750	0.027
Neutrophil	51.223	1.540-1704.069	0.028
Dendritic	2.717	0.563-13.113	0.213
CDH13	0.733	0.647-0.830	< 0.001

Table S4. The correlation between between CDH13 expression and gene markers of immune cells in patients with ccRCC (TIMER)

Immune cells	Gene markers	Correlation adjusted by none		Correlation adjusted by tumor purity	
		r	*p* value	*r*	*p* value
B cell	CD19	-0.151	4.74E-04	-0.162	4.71E-04
	CD79A	-0.134	1.86E-03	-0.162	4.69E-04
	KRT20	-0.214	5.87E-07	-0.239	2.07E-07
CD8+ T cell	CD8A	-0.026	5.56E-01	-0.035	4.49E-01
	CD8B	-0.064	1.41E-01	-0.079	8.98E-02
Dendritic cell	CD1C	0.203	2.21E-06	0.195	2.53E-05
	HLA-DPA1	0.117	6.72E-03	0.105	2.39E-02
	HLA-DPB1	0.063	1.49E-01	0.039	4.07E-01
	HLA-DQB1	0.112	9.87E-03	0.108	2.03E-02
	HLA-DRA	0.08	6.41E-02	0.054	2.44E-01
	ITGAX	-0.153	4.10E-04	-0.167	3.23E-04
	NRP1	0.759	7.28E-101	0.766	4.64E-90
M1 Macrophage	IRF5	-0.265	5.01E-10	-0.287	3.30E-10
	NOS2	0.575	3.74E-48	0.57	5.00E-41
	PTGS2	0.179	3.23E-05	0.186	6.11E-05
M2 Macrophage	ARG1	0.072	9.63E-02	0.064	1.67E-01
	CD163	0.217	4.44E-07	0.169	2.72E-04
	MRC1	0.473	4.03E-31	0.446	6.12E-24
	MS4A4A	0.198	4.28E-06	0.166	3.56E-04
	VSIG4	0.039	3.63E-01	-0.031	5.12E-01
Monocyte	CD86	0.031	4.72E-01	-0.006	8.90E-01
	CSF1R	0.132	2.34E-03	0.094	4.31E-02
Natural cell killer	KIR2DL1	0.334	2.19E-15	0.325	8.69E-13
	KIR2DL3	0.257	1.67E-09	0.229	6.58E-07
	KIR2DL4	0.062	1.50E-01	0.038	4.15E-01
	KIR2DS4	0.258	1.45E-09	0.25	5.59E-08
	KIR3DL1	0.351	6.82E-17	0.341	5.54E-14
	KIR3DL2	0.198	4.23E-06	0.199	1.61E-05
	KIR3DL3	0.056	1.97E-01	0.057	2.24E-01
Neutrophils	CCR7	0.08	6.41E-02	0.051	2.78E-01
	CEACAM8	0.093	3.24E-02	0.096	3.96E-02
	FUT4	0.32	3.53E-14	0.298	6.39E-11
	ITGAM	0.063	1.46E-01	0.034	4.65E-01
T cell (general)	CD2	-0.035	4.24E-01	-0.055	2.36E-01

	CD3D	-0.086	4.66E-02	-0.119	1.03E-02
	CD3E	-0.036	4.04E-01	-0.059	2.10E-01
T cell exhaustion	CTLA4	-0.13	2.67E-03	-0.172	2.11E-04
	GZMB	0.164	1.43E-04	0.142	2.19E-03
	HAVCR2	0.082	5.79E-02	0.058	2.10E-01
	LAG3	-0.176	4.54E-05	-0.188	4.71E-05
	PDCD1	-0.167	1.12E-04	-0.184	7.18E-05
TAM	CCL2	0.169	8.76E-05	0.187	5.59E-05
	CCR5	0.017	7.00E-01	-0.002	9.62E-01
	CD68	-0.049	2.59E-01	-0.075	1.09E-01
	CD80	0.001	9.85E-01	-0.028	5.50E-01
	IL10	0.038	3.83E-01	0.004	9.29E-01
Tfh	BCL6	0.297	2.51E-12	0.287	3.42E-10
	CXCR5	-0.084	5.16E-02	-0.093	4.50E-02
	ICOS	-0.031	4.71E-01	-0.051	2.78E-01
	IL21	-0.056	1.98E-01	-0.066	1.58E-01
Th1	IFNG	-0.107	1.37E-02	-0.135	3.56E-03
	IL13	-0.006	8.84E-01	0.031	5.07E-01
	STAT1	0.084	5.13E-02	0.051	2.72E-01
	STAT4	0.142	9.97E-04	0.126	6.63E-03
	TBX21	0.279	5.33E-11	0.279	1.12E-09
	TNF	-0.025	5.66E-01	-0.063	1.76E-01
Th2	CCR3	-0.132	2.29E-03	-0.146	1.71E-03
	GATA3	-0.005	9.00E-01	-0.015	7.55E-01
	STAT5A	0.03	4.89E-01	0.006	8.94E-01
	STAT6	0.268	3.31E-10	0.27	3.64E-09
Th9	IRF4	-0.084	5.24E-02	-0.108	1.99E-02
	SPI1	-0.136	1.67E-03	-0.17	2.42E-04
	TGFBR2	0.761	5.31E-102	0.766	3.18E-90
Th17	IL-17A	-0.056	2.00E-01	-0.038	4.21E-01
	IL-21R	0.131	2.49E-03	0.109	1.93E-02
	IL-23R	0.009	8.43E-01	-0.023	6.27E-01
	STAT3	0.512	5.68E-37	0.511	5.28E-32
Th22	AHR	0.479	5.61E-32	0.457	3.35E-25
	CCR10	0.243	1.28E-08	0.263	1.05E-08
Treg	FOXP3	-0.158	2.59E-04	-0.189	4.39E-05
	CCR8	-0.023	5.89E-01	-0.031	5.07E-01
	IL2RA	0.142	1.04E-03	0.095	4.09E-02
	STAT5B	0.595	2.83E-52	0.601	1.27E-46
	TGFB1	0.381	6.91E-20	0.369	2.71E-16

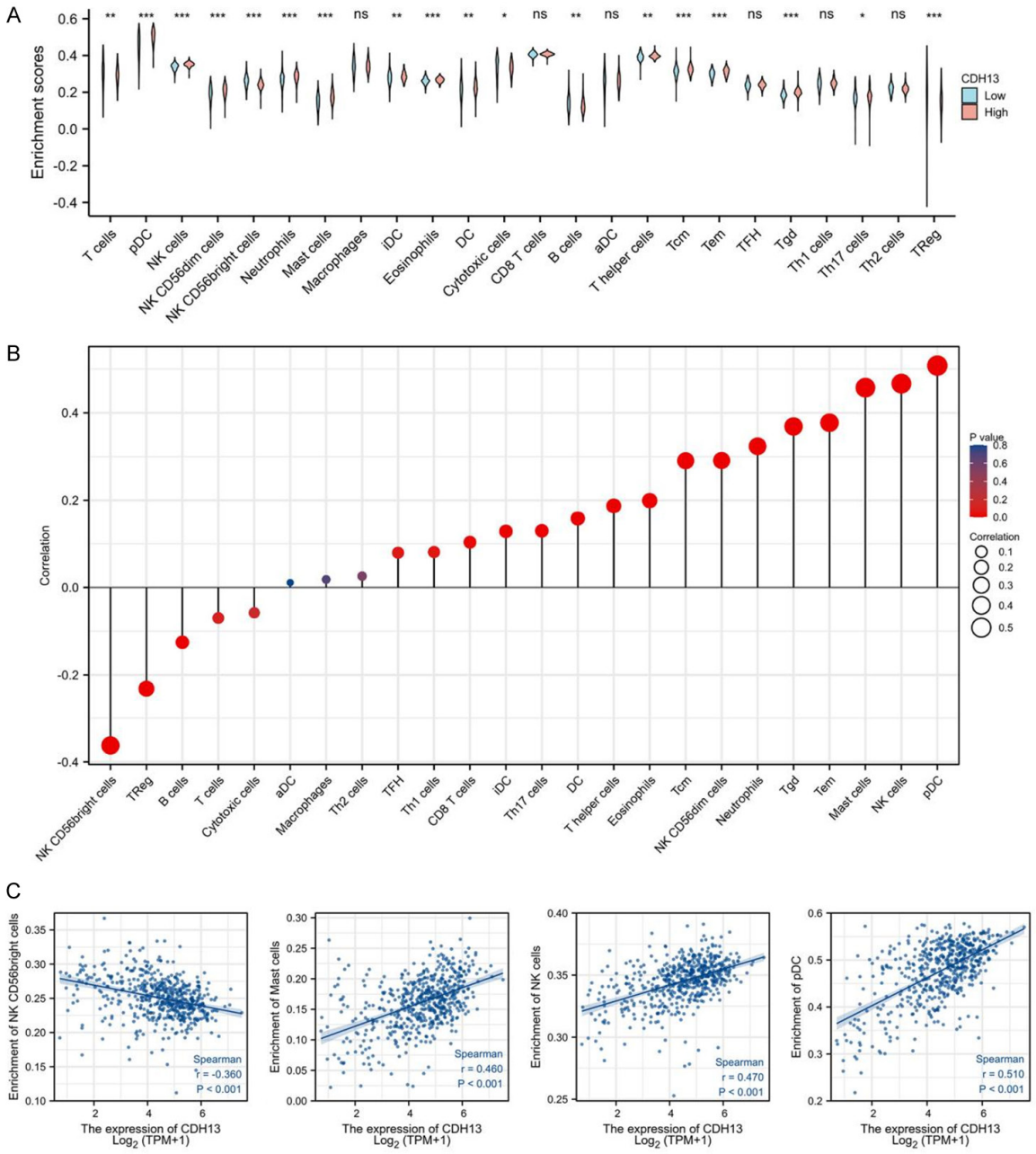

Figure S4. A. The infiltration level of 24 types of immune cells in ccRCC. B. The correlation between CDH13 expression and the infiltration level of immune cells in ccRCC. C. The correlation between CDH13 expression and the infiltration level of NK CD56bright cells, mast cells, NK cells, and pDC in ccRCC.

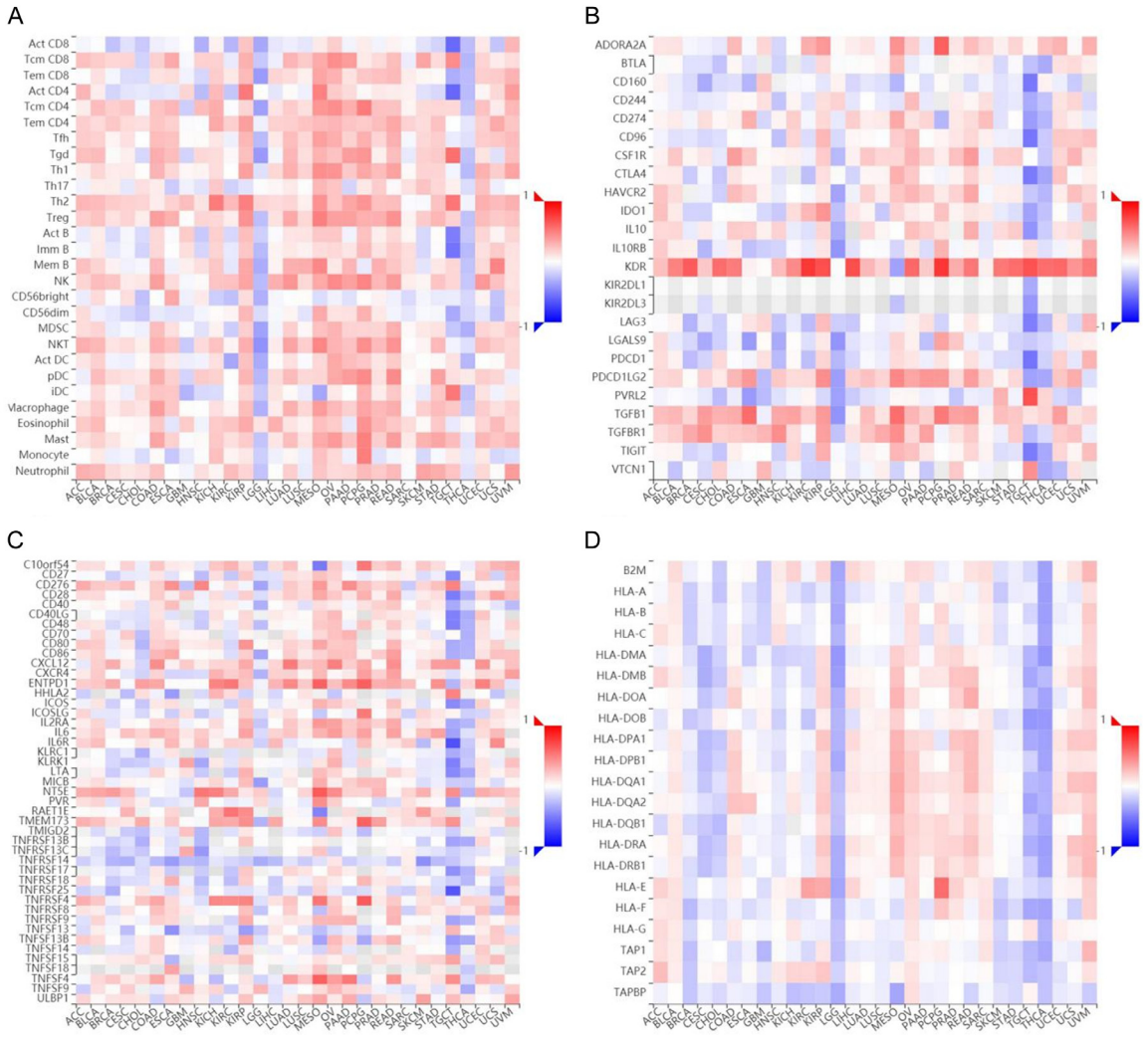

Figure S5. A. Spearman correlation between CDH13 expression and tumor lymphocyte infiltration in ccRCC patients. B. CDH13 expression and immunoinhibitors. C. CDH13 and immunostimulators. D. CDH13 and major histocompatibility complex (TISIDB).

Table S5. The correlation between CDH13 expression and tumor infiltrating lymphocytes in patients with ccRCC (TISIDB)

Factors	*r*	*p* value
Activated CD8 T cell (Act_CD8)	-0.281	4.99e-11
Central memory CD8 T cell (Tcm_CD8)	-0.081	0.0627
Effector memory CD8 T cell (Tem_CD8)	0.092	0.0344
Activated CD4 T cell (Act_CD4)	-0.218	3.89e-07
Central memory CD4 T cell (Tcm_CD4)	-0.01	0.818
Effector memory CD4 T cell (Tem_CD4)	0.184	1.9e-05
T follicular helper cell (Tfh)	-0.058	0.181
Gamma delta T cell (Tgd)	0.029	0.502
Type 1 T helper cell (Th1)	-0.001	0.984
Type 17 T helper cell (Th17)	-0.175	4.69e-05
Type 2 T helper cell (Th2)	0.265	5.45e-10
Regulatory T cell (Treg)	0.074	0.0879
Activated B cell (Act_B)	-0.158	0.000244
Immature B cell (Imm_B)	-0.085	0.0503
Memory B cell (Mem_B)	-0.095	0.0286
natural killer cell (NK)	0.242	1.68e-08
CD56bright natural killer cell (CD56bright)	-0.244	1.29e-08
CD56dim natural killer cell (CD56dim)	0.044	0.31
Myeloid derived suppressor cell (MDSC)	-0.197	4.59e-06
Natural killer T cell (NKT)	0.044	0.314
Activated dendtritic cell (Act_DC)	-0.34	8.39e-06
Plasmacytoid dendtritic cell (pDC)	0.005	0.899
Immature dendtritic cell (iDC)	-0.004	0.926
Macrophage (Macrophage)	0.048	0.263
Eosinophi (Eosinophil)	0.23	8.79e-08
Mast (Mast)	0.125	0.00384
Monocyte (Monocyte)	0.046	0.284
Neutrophil (Neutrophil)	0.261	9.98e-10

Table S6. The correlation between CDH13 expression and immunostimulators in patients with ccRCC (TISIDB)

Factors	*r*	*p* value
C10orf54	0.294	5.48e-12
CD27	-0.217	4.46e-07
CD276	0.117	0.00701
CD28	-0.11	0.0113
CD40	0.074	0.0874
CD40LG	-0.013	0.771
CD48	-0.094	0.0297
CD70	-0.108	0.013
CD80	-0.154	0.000347
CD86	-0.129	0.00274
CXCL12	0.166	0.000123
CXCR4	0.193	6.97e-06
ENTPD1	0.53	< 2.2e-16
HHLA2	0.14	0.00122

ICOS	-0.178	3.6e-05
ICOSLG	0.02	0.65
IL2RA	-0.011	0.8
IL6	-0.024	0.587
IL6R	0.175	4.79e-05
KLRC1	-0.121	0.00511
KLRK1	-0.107	0.0132
LTA	-0.201	2.94e-06
MICB	-0.047	0.274
NT5E	0.377	1.41e-15
PVR	-0.077	0.0768
RAET1E	0.543	< 2.2e-16
TMEM173	0.324	2.28e-14
TMIGD2	-0.127	0.00326
TNFRSF13B	-	-
TNFRSF13C	-	-
TNFRSF14	-0.155	0.000322
TNFRSF17	-0.227	1.21e-07
TNFRSF18	-0.256	2.29e-09
TNFRSF25	-0.108	0.0125
TNFRSF4	0.459	< 2.2e-16
TNFRSF8	0.003	0.946
TNFRSF9	-0.173	6.05e-05
TNFSF13	-0.096	0.0264
TNFSF13B	-0.137	0.00158
TNFSF14	-0.28	5.6e-11
TNFSF15	0.139	0.00132
TNFSF18	-	-
TNFSF4	0.008	0.852
TNFSF9	-0.188	1.27e-05
ULBP1	0.028	0.522

Table S7. The correlation between CDH13 expression and immunoinhibitors in patients with ccRCC (TISIDB)

Factors	*r*	*p* value
ADORA2A	0.316	9.57e-14
BTLA	-0.218	0.00302
CD160	-0.021	0.622
CD244	-0.108	0.0124
CD274	-0.037	0.388
CD96	-0.312	0.00218
CSF1R	-0.059	0.173
CTLA4	-0.247	8.65e-09
HAVCR2	-0.032	0.465
IDO1	0.278	7.67e-11
IL10	-0.122	0.00474
IL10RB	-0.075	0.0831
KDR	0.779	< 2.2e-16
KIR2DL1	-	-

KIR2DL3	-	-
LAG3	-0.257	1.89e-09
LGALS9	-0.125	0.00375
PDCD1	-0.246	9.85e-09
PDCD1LG2	0.144	0.000866
PVRL2	0.039	0.37
TGFB1	0.206	1.72e-06
TGFBR1	-0.019	0.656
TIGIT	-0.173	5.9e-05
VTCN1	-0.18	2.86e-05

Table S8. The correlation between CDH13 expression and major histocompatibility complex in patients with ccRCC (TISIDB)

Factors	*r*	*p* value
B2M	-0.042	0.328
HLA-A	-0.186	1.52e-05
HLA-B	-0.094	0.0293
HLA-C	-0.077	0.0739
HLA-DMA	-0.149	0.000558
HLA-DMB	-0.152	0.000433
HLA-DOA	-0.095	0.0277
HLA-DOB	-0.233	2.17e-07
HLA-DPA1	-0.041	0.345
HLA-DPB1	-0.087	0.0439
HLA-DQA1	-0.075	0.0835
HLA-DQA2	-0.055	0.208
HLA-DQB1	-0.015	0.735
HLA-DRA	-0.087	0.0454
HLA-DRB1	-0.074	0.087
HLA-E	0.57	< 2.2e-16
HLA-F	-0.097	0.025
HLA-G	-0.056	0.197
TAP1	-0.15	0.000528
TAP2	0.164	0.000148
TAPBP	-0.266	1.38e-07

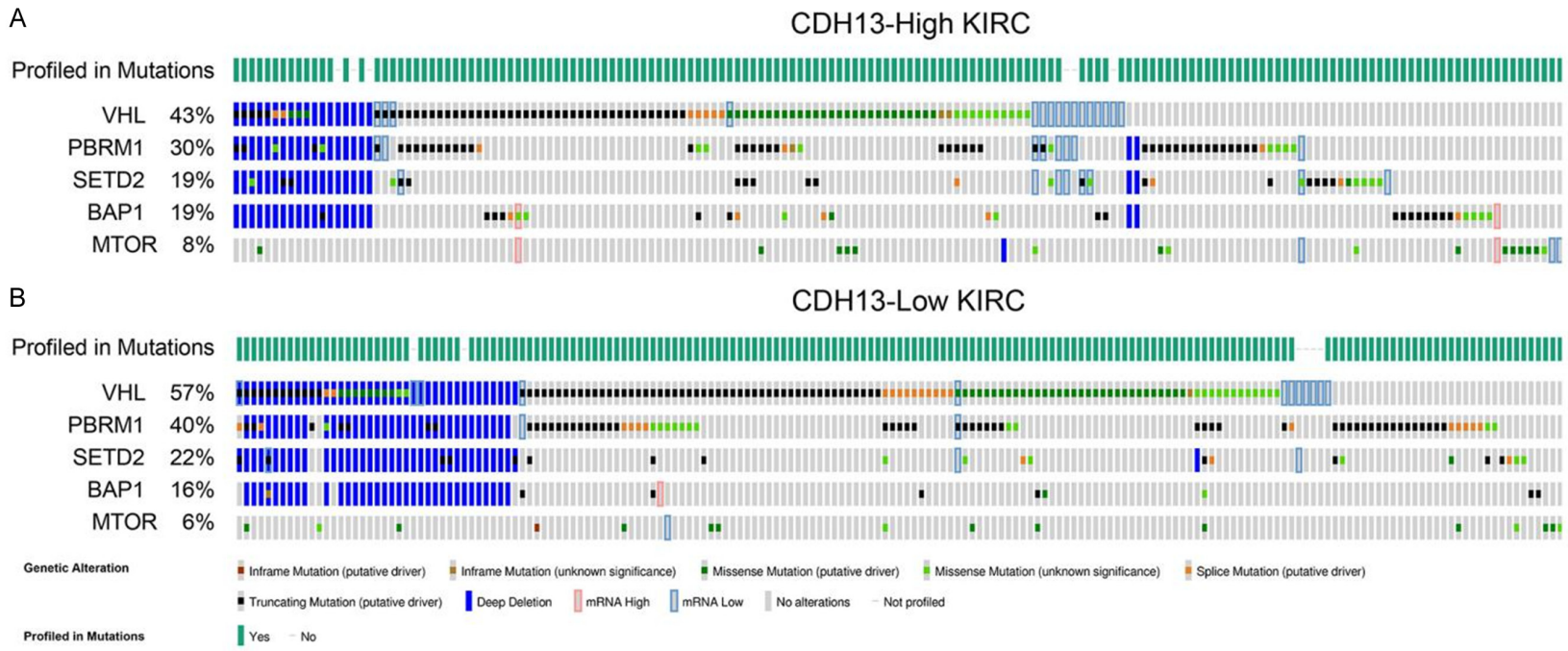

Figure S6. A. VHL, PBRM1, SETD2, BAP1, and MTOR genomic alterations in CDH13-high expression subgroup. B. VHL, PBRM1, SETD2, BAP1, and MTOR genomic alterations in CDH13-low expression subgroup.

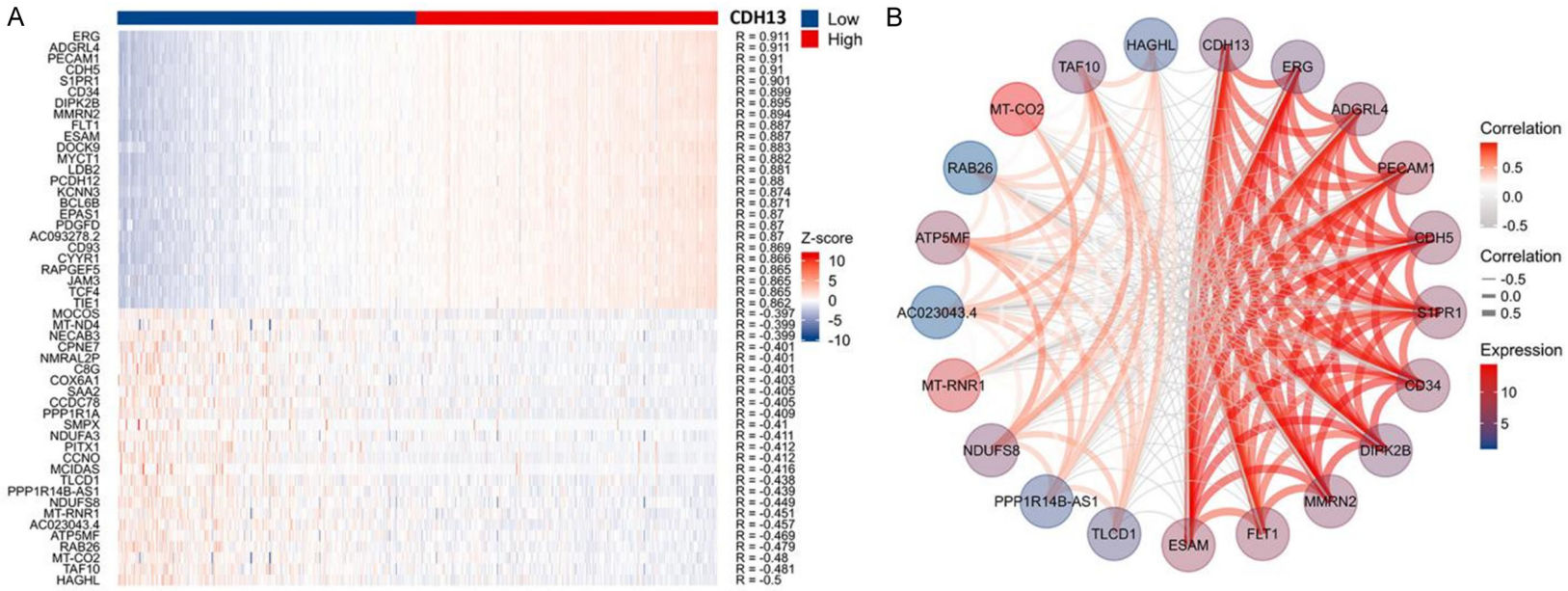

Figure S7. A. Correlation heatmap for the top 25 positively and negatively correlated genes with CDH13 in ccRCC. B. Correlation circle for the top 10 positively and negatively correlated genes with CDH13 in ccRCC.

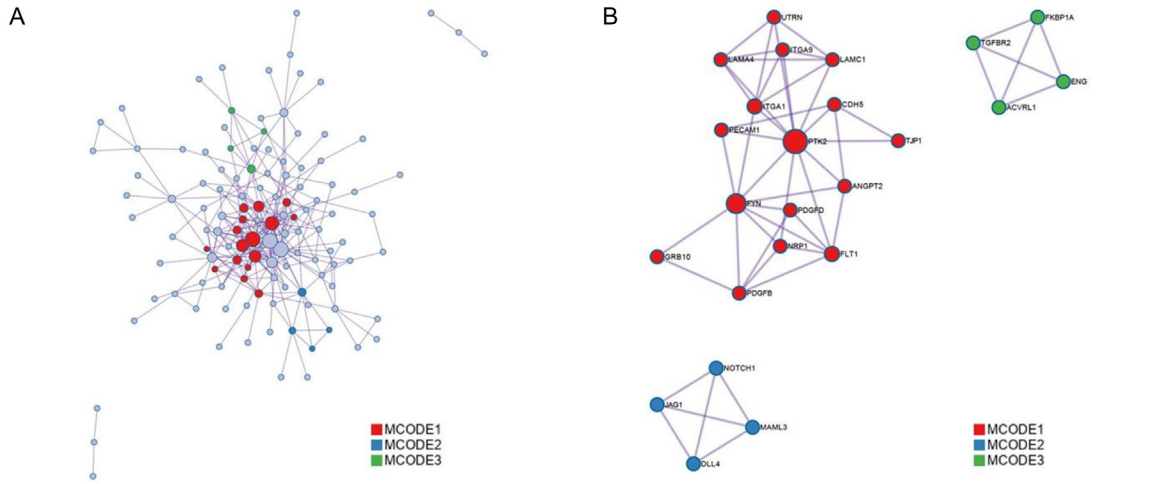

C

Color	MCODE	GO	Description	Log10 (P)
	MCODE_1	ko04510	Focal adhesion	-15.4
	MCODE_1	hsa04510	Focal adhesion	-15.4
	MCODE_1	ko04151	PI3K-Akt signaling pathway	-13.3
	MCODE_2	ko04330	Notch signaling pathway	-11.1
	MCODE_2	hsa04330	Notch signaling pathway	-11.1
	MCODE_2	GO:0045747	positive regulation of Notch signaling pathway	-10.8
	MCODE_3	GO:0048185	activin binding	-13.3
	MCODE_3	GO:0034713	type I transforming growth factor beta receptor binding	-10
	MCODE_3	GO:0005024	transforming growth factor beta-activated receptor activity	-9.5

Figure S8. Protein-protein interaction network and the MCODE components identified in CDH13 and its correlated genes (Metascape).